MASSACHUSETTS INSTITUTE OF TECHNOLOGY
LINCOLN LABORATORY

STUDIES OF THE F-REGION BY THE INCOHERENT BACKSCATTER METHOD

J. V. EVANS

Group 314

TECHNICAL REPORT NO. 274

24 JULY 1962

LEXINGTON MASSACHUSETTS

ABSTRACT

The Millstone Hill radar facility operated by M.I.T. Lincoln Laboratory has made measurements of the distribution of electrons in the F-region of the ionosphere by observing the weak incoherent backscatter signal. These measurements were first made early in 1960 and were continued throughout 1961 on a routine basis at least once a week. This report presents all the electron density profiles measured up to the end of 1961. Results of spectral analyses of the signals made early in 1962 are also given. The distribution of electrons above the peak of the F-region has been a subject of special study. On the basis of the results obtained to date the conclusions reached are: (a) the scale height of the electron density increases with height, (b) the ion temperature is not very dependent on height, though it does show a marked diurnal variation, (c) the electron-to-ion temperature ratio is 1:1 during the hours of darkness, but during the daytime it increases to a peak value $\sim$1.6:1 around noon and (d) the scattering cross section for the electrons is close to the expected value when allowance is made for (c).

TABLE OF CONTENTS

Abstract ii

I. INTRODUCTION 1

II. ELECTRON DENSITY PROFILE MEASUREMENTS 3

A. Methods of Observation and Data Reduction 3

B. The Observations 7

C. Accuracy of the Results 22

D. Discussion of the Results 25

1. General Considerations 25
2. The Height of Maximum Electron Density h_{max} 26
3. Scale Height H_i above h_{max} 26
4. The Total Electron Content of the Ionosphere 33

III. SPECTRUM MEASUREMENTS 34

A. Introduction 34

B. The New Spectrum Analyzer 35

C. Results of Observations in 1962 36

D. Temperature Values 39

E. Summary of the Spectrum Measurements 43

IV. ABSOLUTE SCATTERING CROSS SECTION OF THE ELECTRONS 43

A. Introduction 43

B. The Radar Equation for an Extended Target 44

C. Approximate Radar Equation for a Millstone-Type Antenna 47

D. Values of η_A, η_r and η_s for Millstone Radar 49

E. An Average Value for σ_m 51

F. Summary 54

V. CONCLUSION 54

STUDIES OF THE F-REGION BY THE INCOHERENT BACKSCATTER METHOD

I. INTRODUCTION

The scattering of X-rays by electrons has long been known in classical physics, but only recently has practical use been made of this effect to study the ionosphere. In 1958 Gordon[1] postulated that if a very powerful radar beam were directed at the ionosphere, a weak but detectable echo from the free electrons there might be obtained. Gordon showed that the intensity of the echo can be computed by assuming that the electrons scatter independently, with a scattering cross section σ_e given by the square of the classical electron radius,

$$\sigma_e = \left(\frac{e^2}{mc^2}\right)^2 \quad \text{in Gaussian units} \tag{1}$$

$$= (2.8 \times 10^{-13}\,\text{cm})^2 \quad .$$

Some confusion has arisen because this cross section is defined as that which scatters energy into unit solid angle, whereas, in radar calculations, it is customary to normalize the cross section to correspond to power reflected into 4π solid angle. Hence the radar cross section of the electrons is $4\pi\,\sigma_e$. For a volume containing N electrons the phases of the N reflected waves will be independent, and the powers should add to give a scattered power proportional to $N\,\sigma_e$. This conclusion can be reached by following the original work of Lord Rayleigh[2] on the behavior of independent oscillators. Alternatively, one can arrive at the same result by considering the electron gas a plasma in which there are small instantaneous changes of the dielectric constant due to the random motion of the electrons. In this case the reflection can be considered to arise as a consequence of irregularities in the refractive index of the medium. Again it is found[3] that the echo power should be proportional to the electron density N.

Gordon[1] predicted that because the electrons would completely fill the beam of the radar, the echo power should vary with range R only as $1/R^2$, not $1/R^4$ as for conventional, i.e., "point" targets. In addition, he speculated that the echo power would exhibit a Doppler-broadened spectrum (in the region of 100 kcps for a wavelength of 1.5 m) because of the random thermal motions of the electrons. Thus, since the echo power would be distributed over a wide range of frequencies, it would be difficult to detect.

The first successful experimental observations came later in 1958 when Bowles[4] succeeded in detecting the echoes by use of a radar operating at a frequency of 41 Mcps. This equipment employed a transmitter with a peak pulse output of about 1 Mw, together with an aerial system which took the form of a linear array covering an area of about one acre. Bowles[5] made the important discovery that, contrary to the predictions of Gordon,[1] the echo spectrum was very

narrow. He correctly attributed this to the presence of the ions in the plasma that control the macroscopic density variations of the electrons. That is, the electrons which have a high mobility compared to the ions are compelled by coulomb forces to move in a way which will keep any part of the plasma electrically neutral. The range of these coulomb forces is characterized by the Debye length λ_D given in

$$\lambda_D^2 = \frac{kT}{4\pi Ne^2} \quad , \tag{2}$$

where k is Boltzmann's constant, T is the electron temperature, N is the electron density and e the charge of an electron. In most parts of the ionosphere, λ_D is of the order of a few millimeters, i.e., much shorter than the wavelength of the exploring wave. As a result, the wave is sensitive to the density fluctuations in the electron gas impressed by the motion of the ions. Bowles[5] modified Gordon's[1] theory to take this effect into account by postulating that the scattering could be considered the result of an imaginary particle having the cross section of an electron and the thermal velocity of an ion. The spectrum of the echo power would still be characterized by a Gaussian function, but one which is some two orders of magnitude narrower than predicted by Gordon.[1]

More recent theoretical investigations of this problem by Fejer,[3,6] Farley, et al.,[7] Dougherty and Farley,[8] Hagfors[9] and Salpeter[10,11] have shown that this view is not strictly correct. A complete treatment of the problem of the electron-ion interactions shows that the strength of the returned signal should be only half that predicted by Gordon,[1] and further, that the shape of the spectrum is not Gaussian, but flat-topped with "wings" at the edges. The theoretical form of this spectrum is shown in Fig. 1, together with the Gaussian profile for comparison. The wings of the

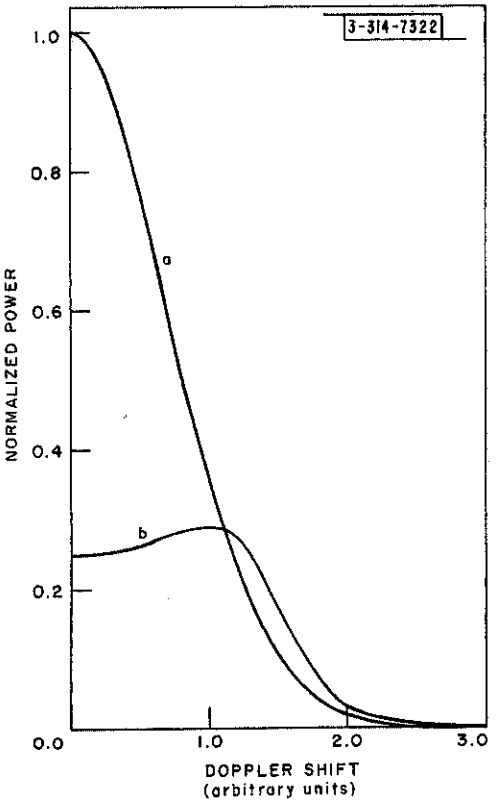

Fig. 1. The normalized power spectrum of thermal density fluctuations (a) for a collisionless gas of neutral particles of mass m_i, and (b) for the electrons in a collisionless plasma in which the ions have mass m_i. Curve (a) has the same shape as the power spectrum suggested by Gordon[1] who supposed that m_i was the mass of an electron, thereby giving a spectrum much wider than (b) (after Dougherty and Farley[8]).

spectrum correspond roughly to the Doppler shift introduced by electrons moving at the velocity of sound for the ions. Thus, the spectrum resembles that which would be caused by greatly damped sound waves in the medium. The electrons may be thought of as having two motions. One is their own thermal motion, which, being higher than that of the ions, would cause a very wide range of Doppler broadening. The second motion is impressed by the more slowly moving ions by means of coulomb forces. This second motion gives rise to a narrow echo spectrum centered at the radio frequency.

The discovery of the narrow form of the central part of the spectrum makes it possible to measure these echoes with an antenna considerably smaller than the one (300 meters in diameter) proposed by Gordon. Thus, the Millstone Hill radar can be used for these measurements.

Observations of incoherent backscatter as a means of studying the ionosphere commenced at Millstone Hill early in 1960, under the direction of Mr. V.C. Pineo. Since that time several reports on particular aspects of the work have appeared.[12-15] Most of these reports deal with small sections of the results, and no paper presenting all the available data has yet been published, though one report[16] did review the electron density measurements made in winter, when the best results are obtained. The present paper provides an account of all the electron density measurements made up to the end of 1961. Preliminary results of some spectrum measurements made early in 1962 are also included. Since these two topics represent different phases of the work, they will be presented and discussed separately.

II. ELECTRON DENSITY PROFILE MEASUREMENTS

A. Methods of Observation and Data Reduction

The Millstone Hill radar facility is located near the town of Westford, Massachusetts (71.5°W, 42.6°N). Observations from this site, therefore, are related solely to the behavior of the ionosphere at northern temperate latitudes. The facility has been described in some detail by Pettengill and Kraft[17] and Arthur, et al.[18] so that the description of the equipment given here will be confined to a table of the equipment parameters (Table I). The choice of some of the parameters in Table I is not obvious and calls for comment. The pulse length (500 μsec) employed for most observations corresponds to a very large height interval (75 km) when the antenna is directed vertically upward. The electron density profile observed under these conditions would be the convolution of the true density profile with a square pulse 75 km in length. Since 75 km is as large as or larger than the scale height of the ionization at the peak of the F-region, such a long pulse yields a very distorted density profile for all heights below about 500 km. Above this height, the ionization density decays with a scale height of $\geqslant$150 km, and the finite width of the pulse ceases to distort the density profile greatly. The use of a shorter pulse would permit a better examination of the region of peak electron density but would yield less echo power, since the echo intensity is proportional to the pulse length. Thus, some compromise between resolution and echo intensity must be sought. In most of the work at Millstone Hill, a fixed 500-μsec pulse was used, and improved resolution of the regions below 500 km was obtained by reducing the antenna elevation so that the intersection of the ray path and the ionospheric layers became more obtuse. An alternative approach would be to keep the antenna pointed at the zenith and make observations with a variety of pulse widths, but this procedure would call for corresponding changes in the receiver bandwidth.

For most observations a receiver bandwidth of 11 kcps was employed, although experiments also were conducted using both narrower and wider receiver bandwidths. A receiver matched

TABLE I

EQUIPMENT PARAMETERS OF THE MILLSTONE HILL RADAR

Parameter	Measurement
Location	71.5°W, 42.6°N
Frequency	440 Mcps (68-cm wavelength)
Antenna	84-ft parabola with conical horn feed
Effective antenna aperture	$210 \pm 10\ m^2$
Antenna gain	37.5 ± 0.5 db
Beamwidth	2.1°
Polarization	right circular (transmitted) left circular (received)
Peak transmitted power	2 to 2.5 Mw
Pulse length	500 μsec (for these observations)
Pulse repetition frequency	50 pps (for these observations)
Receiver bandwidth	11 kcps
Receiver noise figure	3 db (approximately)
Over-all feeder losses	2 db (approximately)
Input signal-to-noise ratio improvement through video integration	generally 20 db

to a 500-μsec pulse would require a bandwidth of only 2 kcps, but a wider filter width is required as a consequence of the Doppler broadening of the signals. The early spectrum measurements of Pineo, et al.[12, 13] and the more precise ones reported in this paper indicate that, for most of the day, the spectral width of the signals is about 11 kcps for all F-region heights. A filter which provides an approximate match to this signal is employed in the receiver.

The available transmitter power and the operating wavelength (68 cm) are dictated by the design of the transmitter system and cannot readily be changed. The polarization of the transmitted wave, however, can readily be altered, although in most measurements right-handed circularly polarized waves were transmitted and left-handed waves received. No signals could be detected when right-handed waves were both transmitted and received. Millman, et al.[19] have reported backscatter observations where linearly polarized waves were employed, and use was made of the Faraday effect in the earth's ionosphere to introduce fading in the signals. These measurements enable one to compute total numbers of electrons between given height intervals. Similar measurements have not been undertaken at Millstone Hill, because they are more difficult to interpret and the results are generally less useful.

The signals observed are exceedingly weak, and at best the predetection signal-to-noise ratio of the echo corresponding to the peak of the F2-region rarely exceeds 1:1. At other heights the echo is always weaker than the receiver noise. On winter nights, when the F-region critical frequency drops to a low value, good results are unobtainable. In summer, echoes can be obtained during both the day and the night, but the quality of the results is generally poor compared with that obtained on winter days, when the critical frequency is at its highest.

In order to obtain any useful results, a considerable amount of video integration is required. This is accomplished in the following way. The output of the matched filter in the receiver is

rectified by using a square-law detector. The resulting voltage (which is proportional to the received power) is sampled by means of a digital voltmeter and assigned one of 256 possible levels. A "word" representing this level is then transmitted to the CG-24 computer and stored. The samples are made at delay intervals of 250 μsec along each sweep of the radar time base. The samples are synchronized with the transmitter repetition frequency so that they are taken at the same points along the time base on each sweep. The words can then be added together in the computer to determine the average power at each given delay. Generally, this integration process is continued for a period of 5 minutes (15,000 sweeps), thereby improving the sensitivity of the system by an amount equivalent to 20.8 db in the predetector signal-to-noise ratio. The integration process is drift-free and can be continued almost indefinitely, although it is rarely continued for longer than 15 minutes. Various forms of external interference* make several short runs preferable to one long one. At the completion of an integration, the sums of the samples are displayed on an oscilloscope [Fig. 2(a)] and printed out on punched paper tape for later analysis. This process requires less than a minute to complete. Figure 2(a) shows the summation of the samples taken with an antenna elevation of 15° for a five-minute period beginning at 1443.5 EST on 7 October 1961. The vertical line has no special significance. At the lower left corner of the picture can be seen four dots which represent the base line. These are samples obtained during the transmitter pulse when the receiver was gated off. The spike which follows the gated portion is caused by ground clutter, which usually extends out to ranges of 200 km and prevents observations of the E-region when the antenna is at the zenith. Beyond the ground clutter can be seen the echoes from the ionosphere – first the E-region and then the F2-layer. The square pulse further along the time base is a calibration pulse caused by introducing (via a directional coupler) a pulse of broadband noise into the receiver on each sweep of the time base. The calibration pulse represents a 100°K increase in the effective receiver temperature. From the height of this pulse relative to the height of the mean noise level, one can conclude that (in this instance) the effective receiver temperature was about 620°K and that the signal-to-noise ratio of the echo corresponding to the peak of the F2-region is about −7 db. These numbers are required if the density of the electrons must be computed absolutely.

When the punched paper tape is used as an input to the CG-24 computer, the numbers representing the points in Fig. 2(a) are printed out. The computer also reduces the measurements to an electron density vs height profile in the following way. First, the mean of all the samples in which only receiver noise was measured is obtained. This process is somewhat subjective since it requires the computer operator to move the vertical line in Fig. 2(a) beyond the F-region echo so that this will not be included in the averaging, but the chance of error is small. The mean receiver noise power is then subtracted from all the samples. The range R corresponding to each sample is next computed and each sample is scaled up by an amount proportional to the square of its range (R^2). Finally, the height corresponding to each sample is computed, with allowance being made for the elevation of the antenna and the curvature of the earth. These reduced data points are displayed in Fig. 2(b) and printed out in the form of a table. Figure 2(b) shows electron density (measured vertically along the ordinate) plotted as a function of height (measured along the abscissa). The R^2 factor considerably increases the importance of the

* A particularly vicious variety is the interference produced by certain aircraft which carry radio altimeters tuned near the radar frequency.

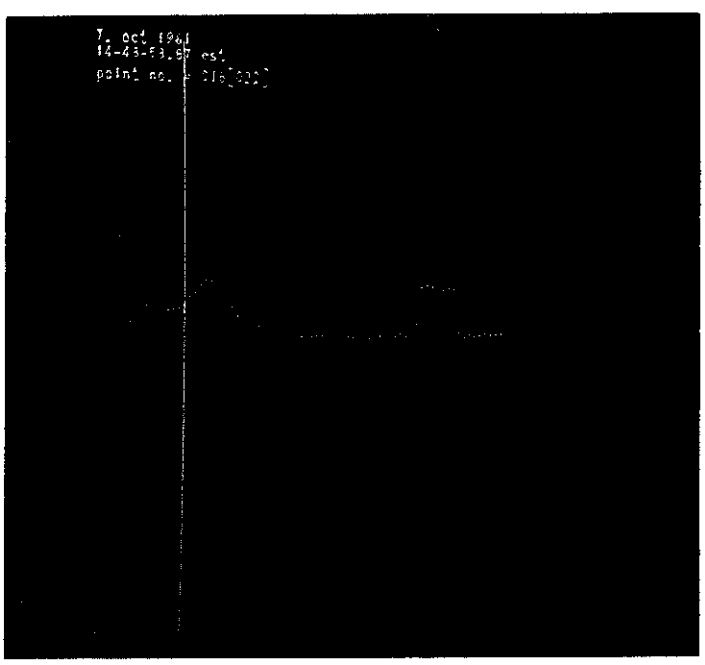

-314-7323(a-b)

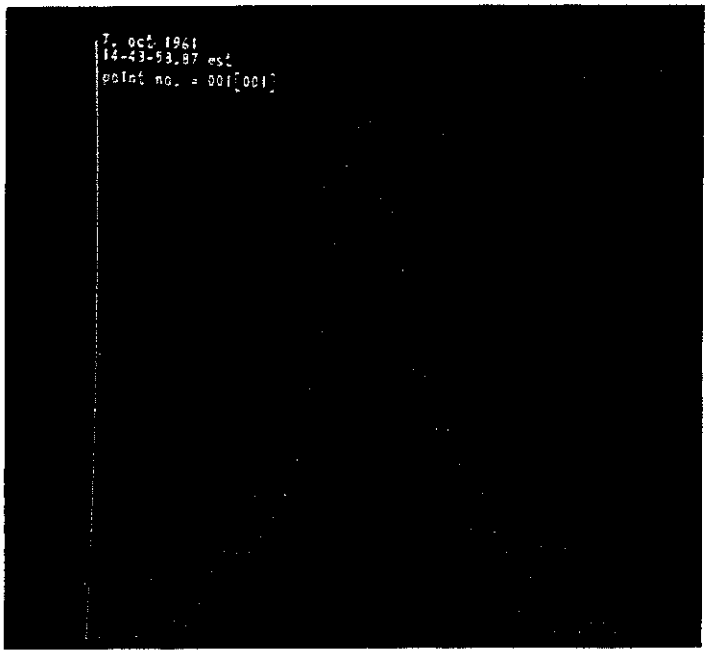

Fig. 2(a-b). In (a) the observed echo power as a function of range is shown after five minutes' integration. The square pulse toward the end of the time base is a calibration signal. The points in (b) represent the electron density (along the ordinate) as a function of height obtained from the data in (a).

F2-region in relation to the E-layer. Also, the errors associated with the points become progressively larger at greater altitudes, as can be seen by the increased scatter of the points.

B. The Observations

During 1960 observations were made for the purpose of certain special investigations (e.g., to measure the signal spectrum) rather than on a routine basis. Thus, only 19 profiles obtained in 1960 were suitable for inclusion. The remainder of the results were obtained in 1961 when observations were made weekly (or sometimes biweekly), though some measurements proved valueless because of equipment malfunctions which were not recognized during the measurements. One unfortunate aspect of the work reported here is that no systematic way of taking the measurements seems to have been established until the middle of 1961. Prior to that time the experimental method was dictated by the particular investigation in progress. Thus, observations were made with receiver bandwidths of 2, 5 and 40 kcps in addition to the 11-kcps bandwidth generally used. Also, no specific set of antenna elevations was employed. During many observation periods measurements were taken only in the zenith, and these measurements yield inaccurate density profiles (Sec. II-A). Therefore, on each of the profiles (Figs. 3 through 16) the receiver bandwidth and antenna elevation are stated. Profiles obtained with a 2-kcps bandwidth and/or only in the zenith (elevation = 90°) are likely to be in considerable error in the region of peak electron density.

During the latter half of 1961, the following method of taking measurements was established:

(1) The receiver bandwidth was set at 11 kcps.

(2) A pulse length of 500 μsec and a pulse repetition frequency of 50 cps were employed.

(3) Two five-minute runs were made at each of the elevations 90°, 45° and 15°.

Although the data obtained in this fashion extend over a period of about 40 minutes, they are used to obtain a single electron density profile. A mean was taken of the two runs at each elevation, and the three sets of points corresponding to the three elevations were then plotted (Fig. 17). A mean curve was drawn so that it fitted the points obtained at 15° elevation to a height of about 400 to 500 km. Beyond this, greater weight was given to the points taken at 45° and 90° elevation. Although not all the profiles presented in this report contain so many experimental points, most represent the mean of two or more five-minute runs. On each profile the time interval over which the measurements were made is stated.

In order to present the profiles in a uniform manner it is convenient to normalize the electron density with respect to the peak of the F2-layer. On two profiles, Figs. 12(a-b), the F2 peak was not the greatest electron density observed, because strong sporadic E-echoes were obtained. In these instances, the density was again normalized to the F2-region peak, but the scale on the abscissa was changed. Because the results are presented in this normalized fashion, there is little need for the absolute electron density to be derived from a knowledge of the echo power and the equipment parameters. Indeed, since such measurements are only accurate to ±20 percent, it is more convenient to establish the absolute electron density at one height, generally the peak of the F2-region, by means of ionosonde data. Shown on each of the profiles is f_oF2, together with f_oE, and f_oE_S where appropriate. For the early measurements in 1960, values of the critical frequencies observed at Ft. Belvoir, Virginia (77.5°W, 39.0°N), have been used and these are indicated by a "B" in parentheses. The data used are the hourly values closest to the time

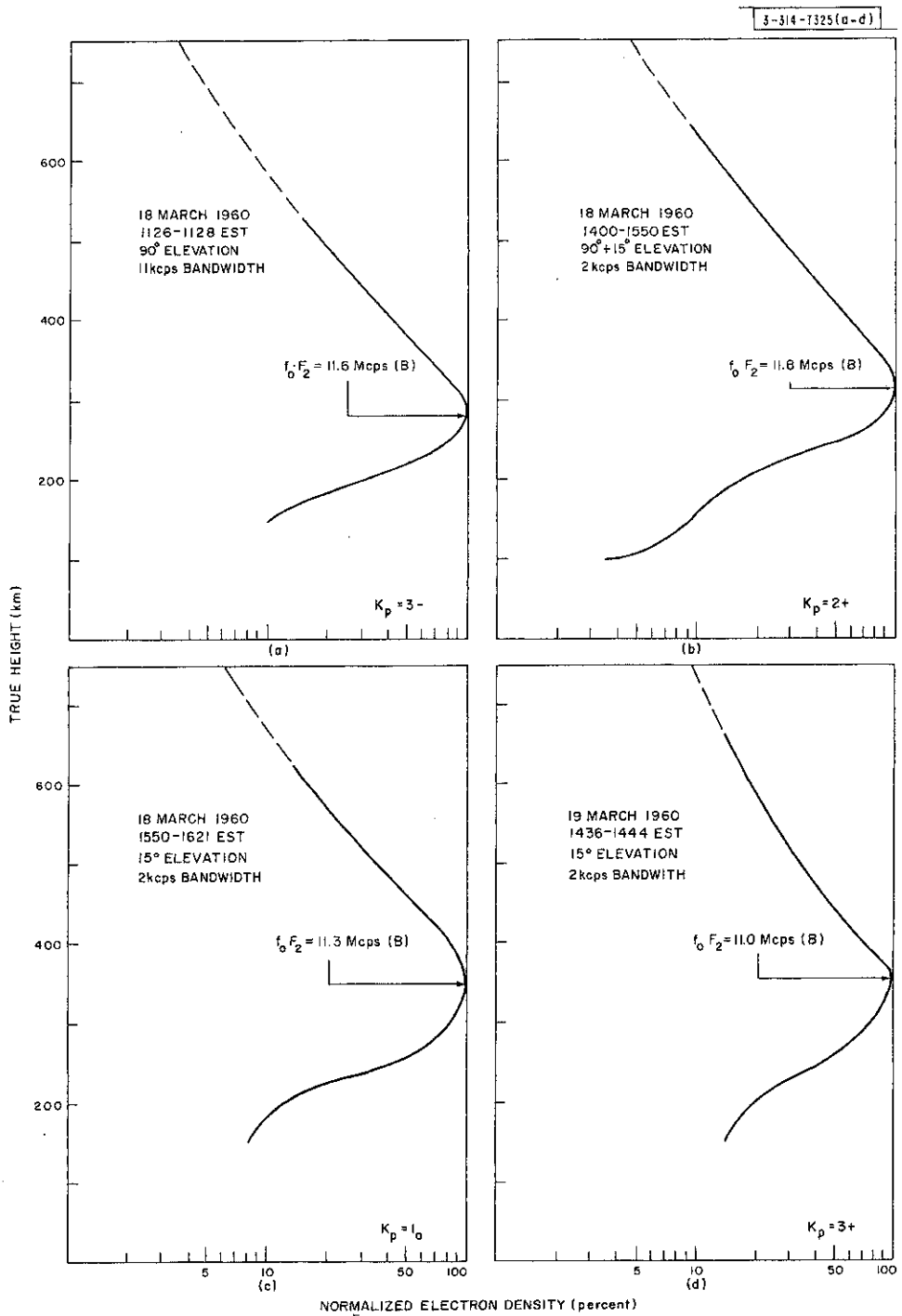

Fig. 3(a-d). Electron density profiles observed by means of the incoherent backscatter technique at Millstone Radar.

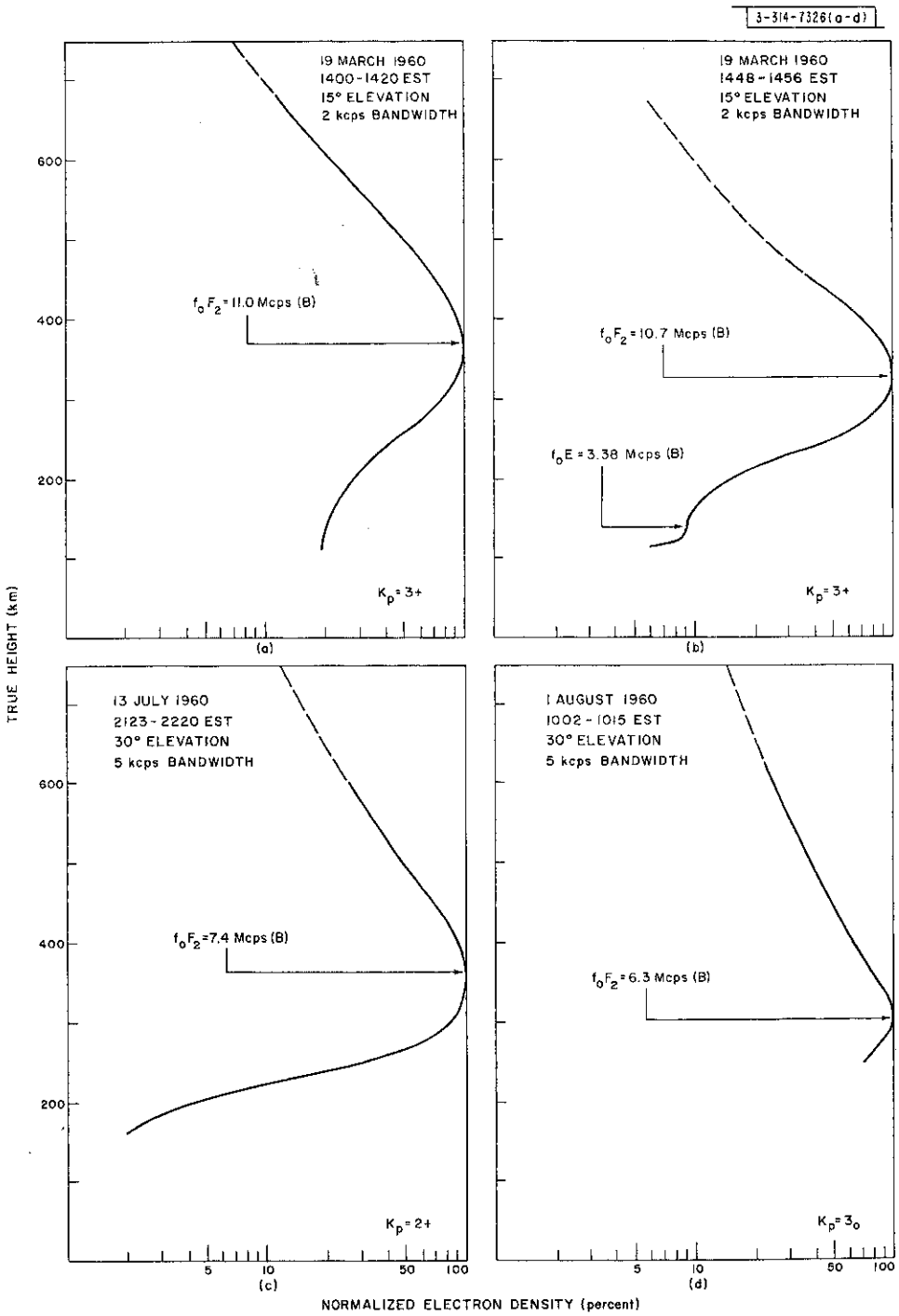

Fig. 4(a-d). Electron density profiles observed by means of the incoherent backscatter technique at Millstone Radar.

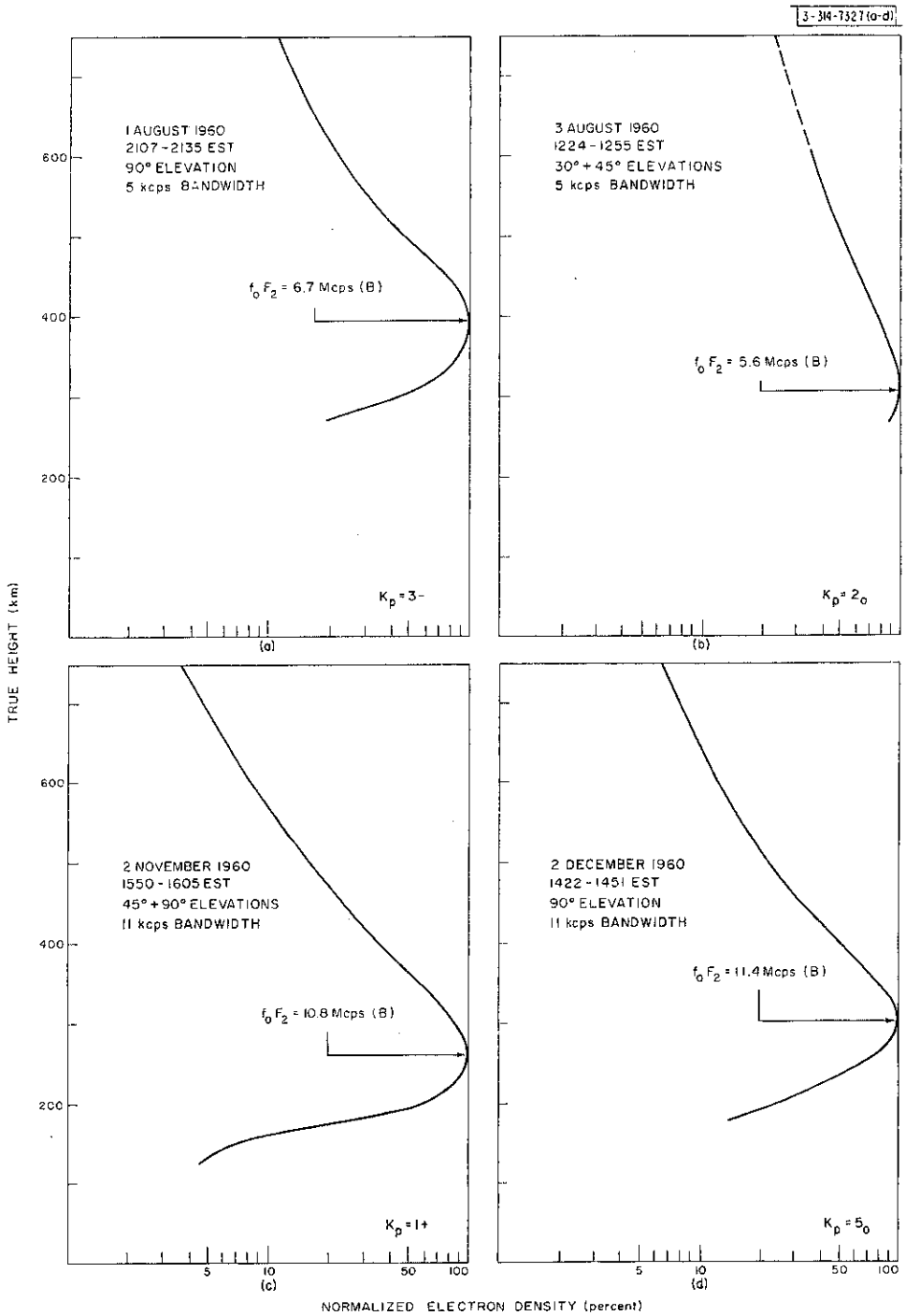

Fig. 5(a-d). Electron density profiles observed by means of the incoherent backscatter technique at Millstone Radar.

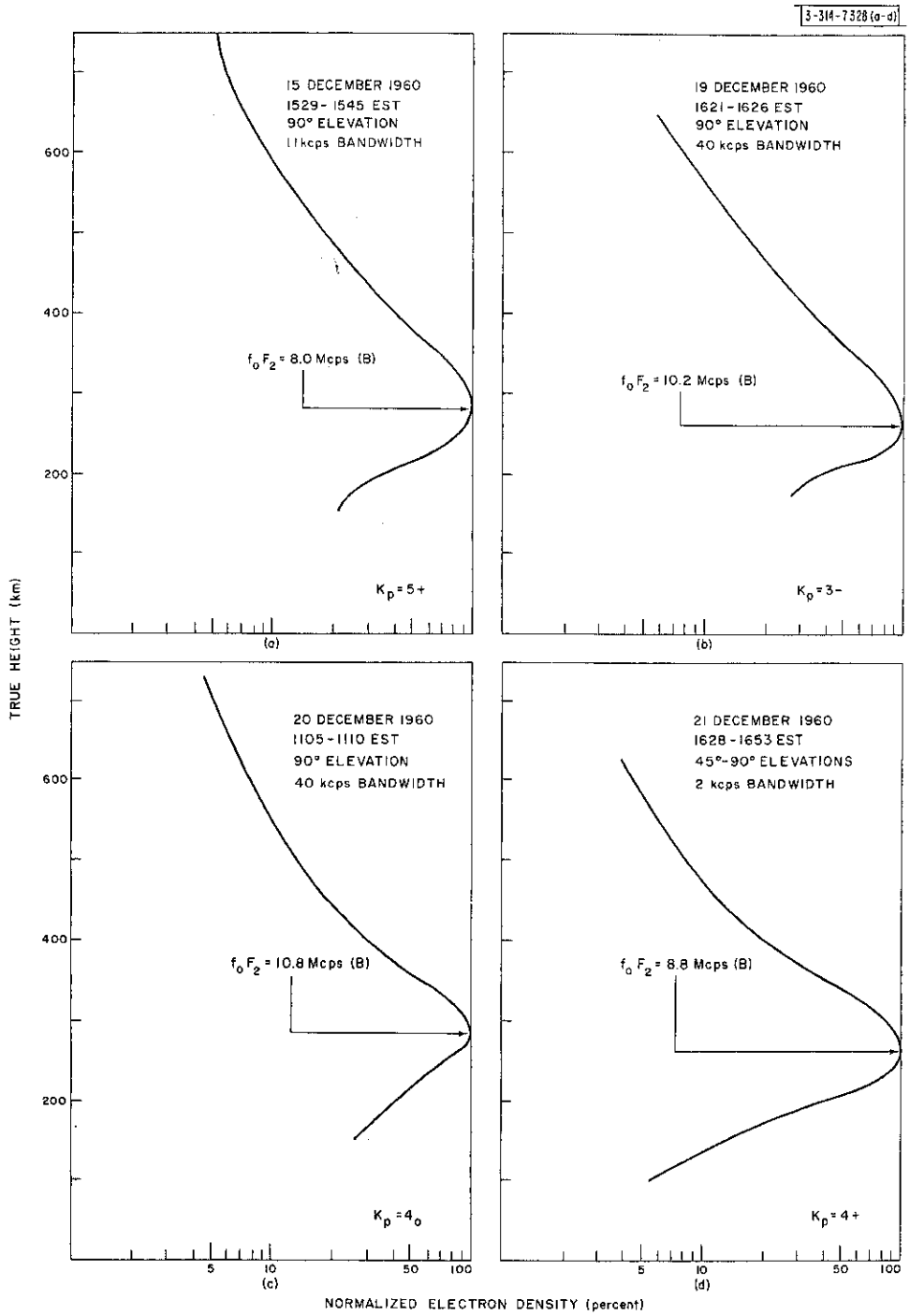

Fig. 6(a-d). Electron density profiles observed by means of the incoherent backscatter technique at Millstone Radar.

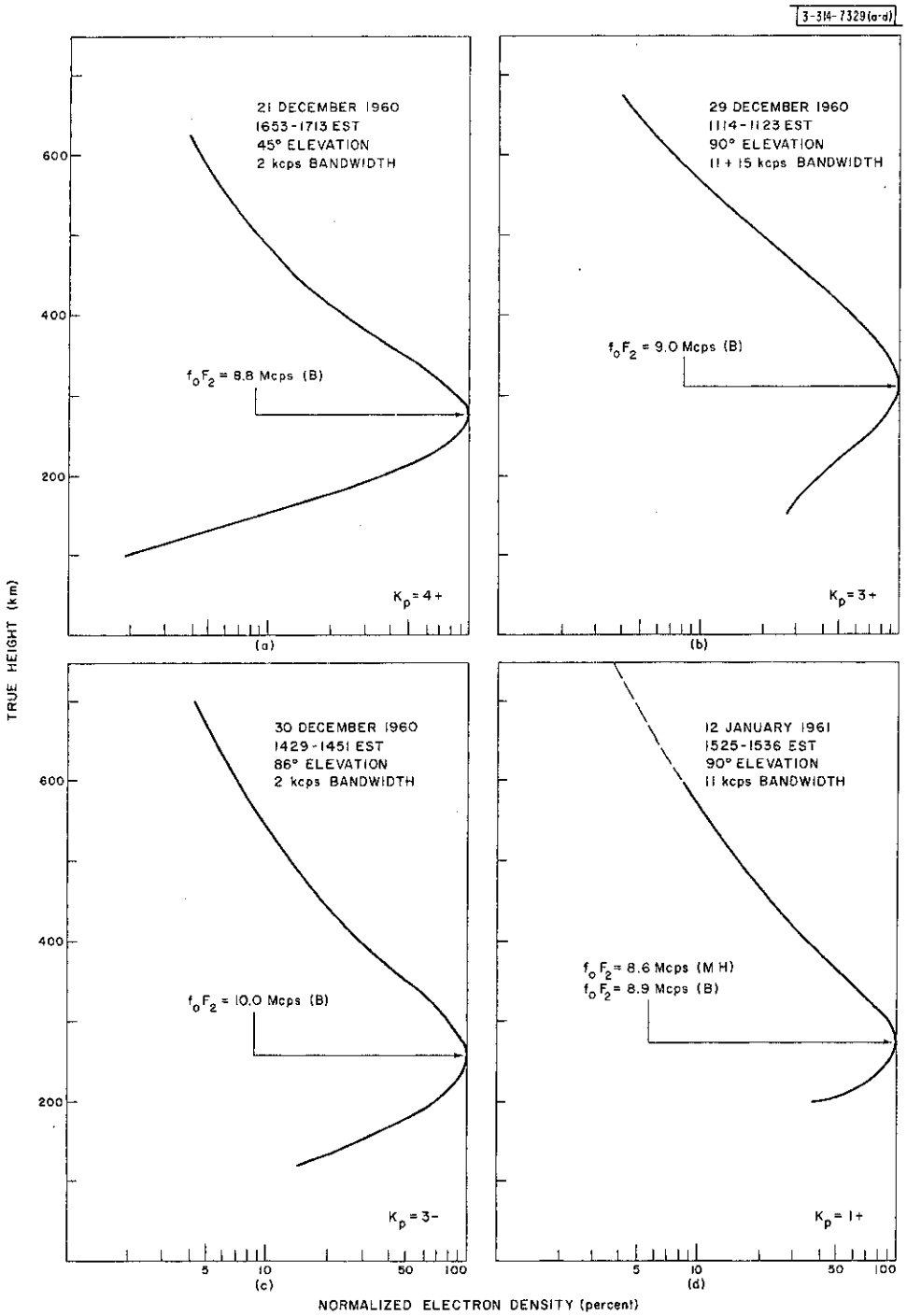

Fig. 7(a-d). Electron density profiles observed by means of the incoherent backscatter technique at Millstone Radar.

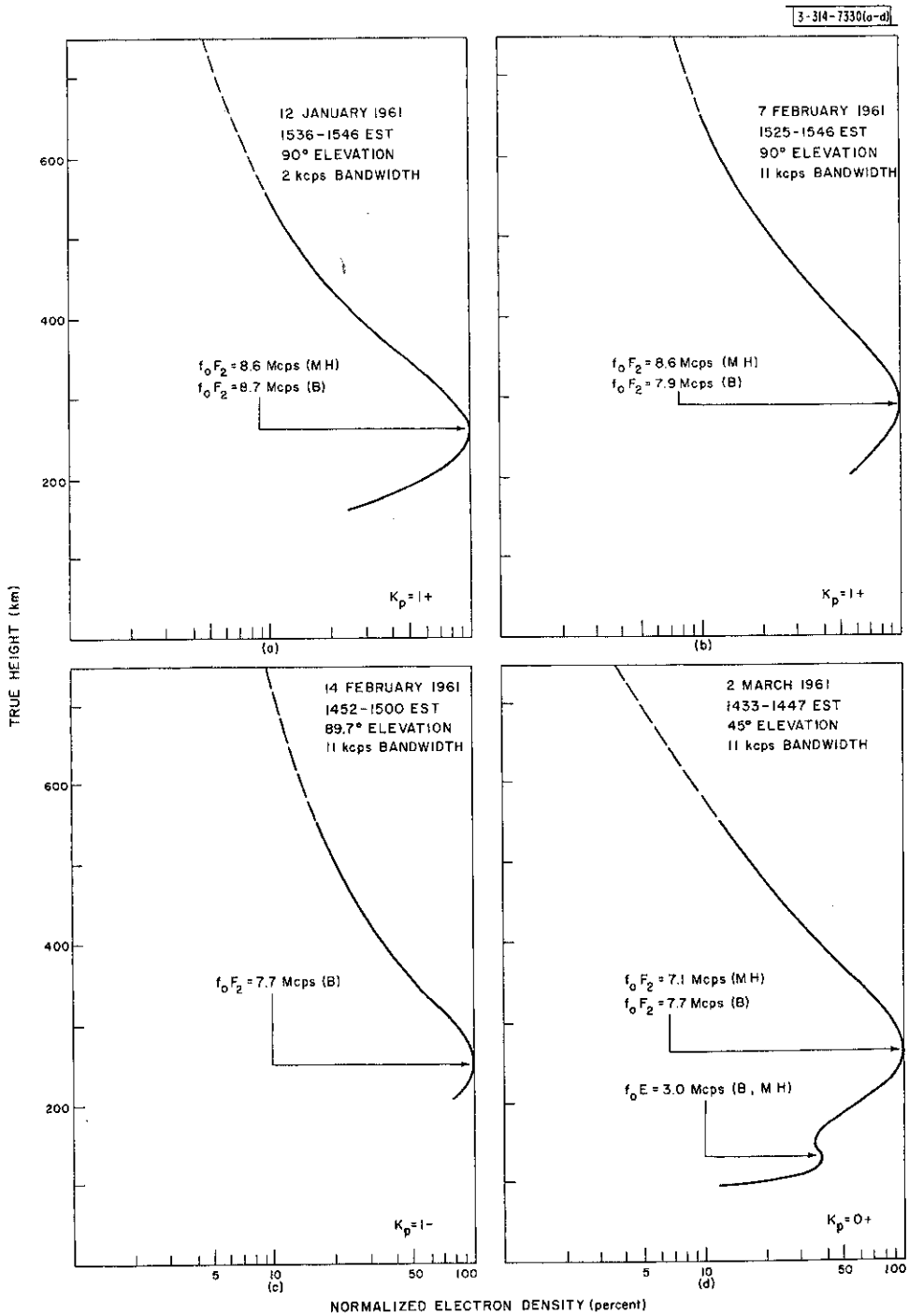

Fig. 8(a-d). Electron density profiles observed by means of the incoherent backscatter technique at Millstone Radar.

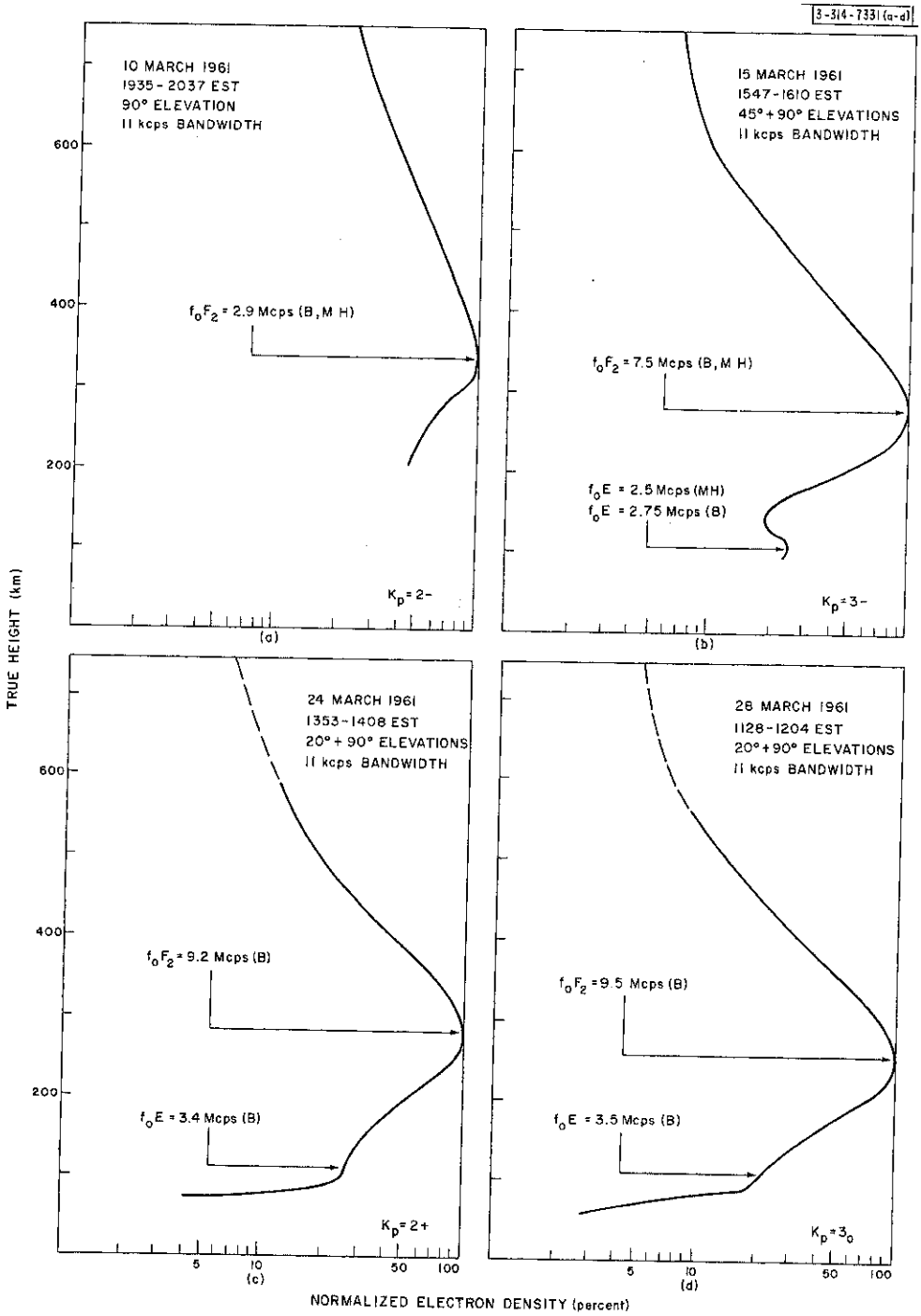

Fig. 9(a-d). Electron density profiles observed by means of the incoherent backscatter technique at Millstone Radar.

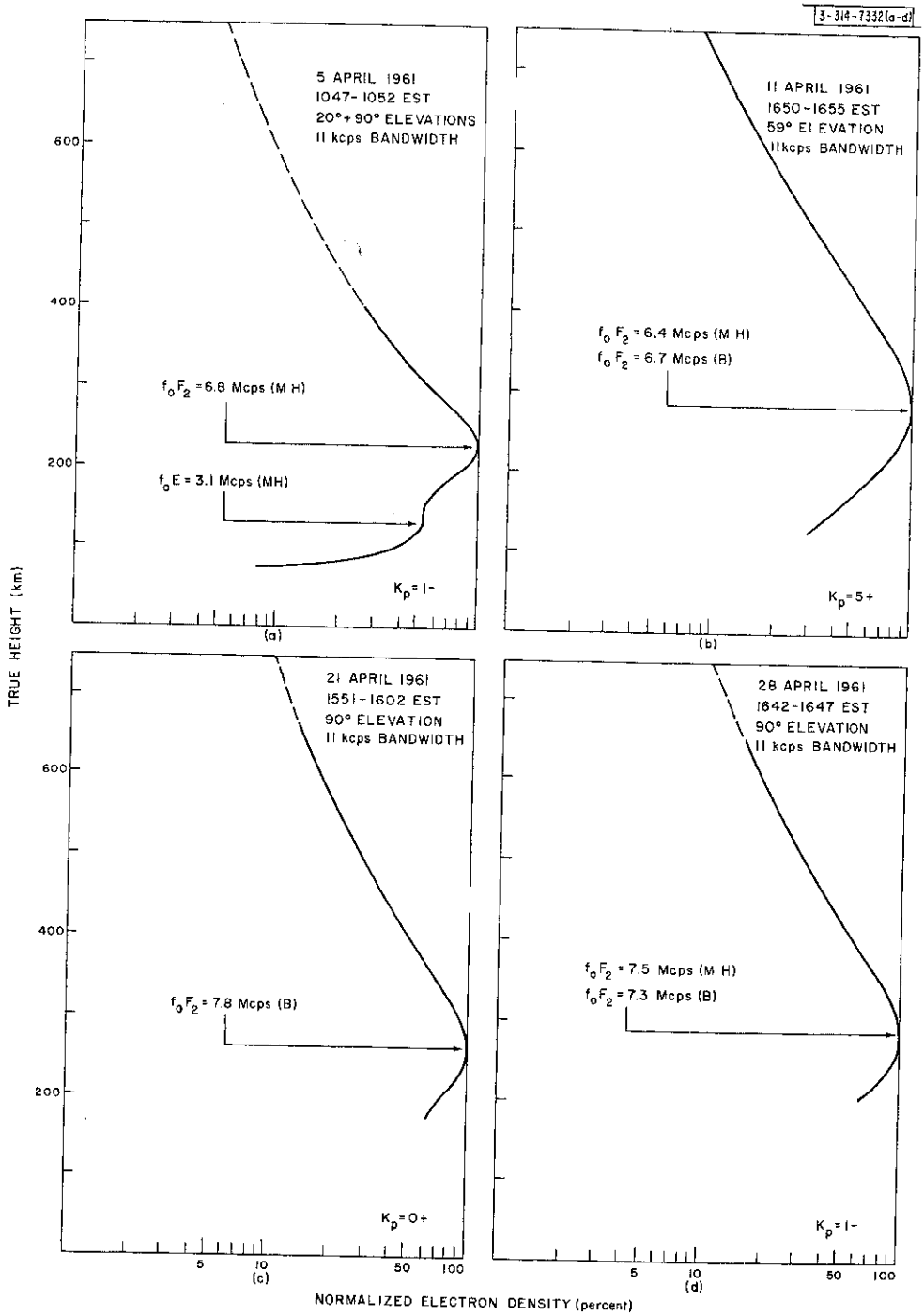

Fig. 10(a-d). Electron density profiles observed by means of the incoherent backscatter technique at Millstone Radar.

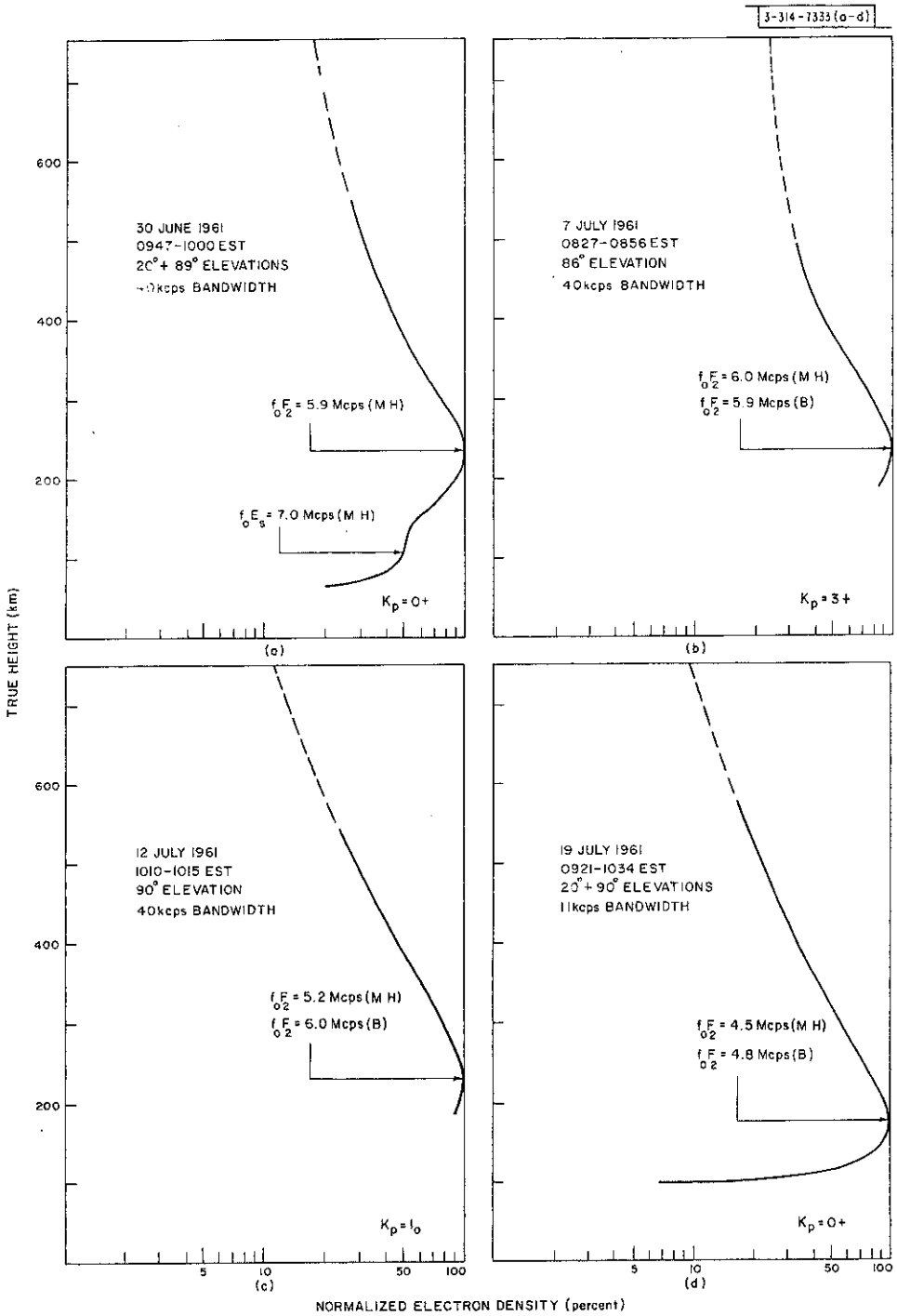

Fig. 11(a-d). Electron density profiles observed by means of the incoherent backscatter technique at Millstone Radar.

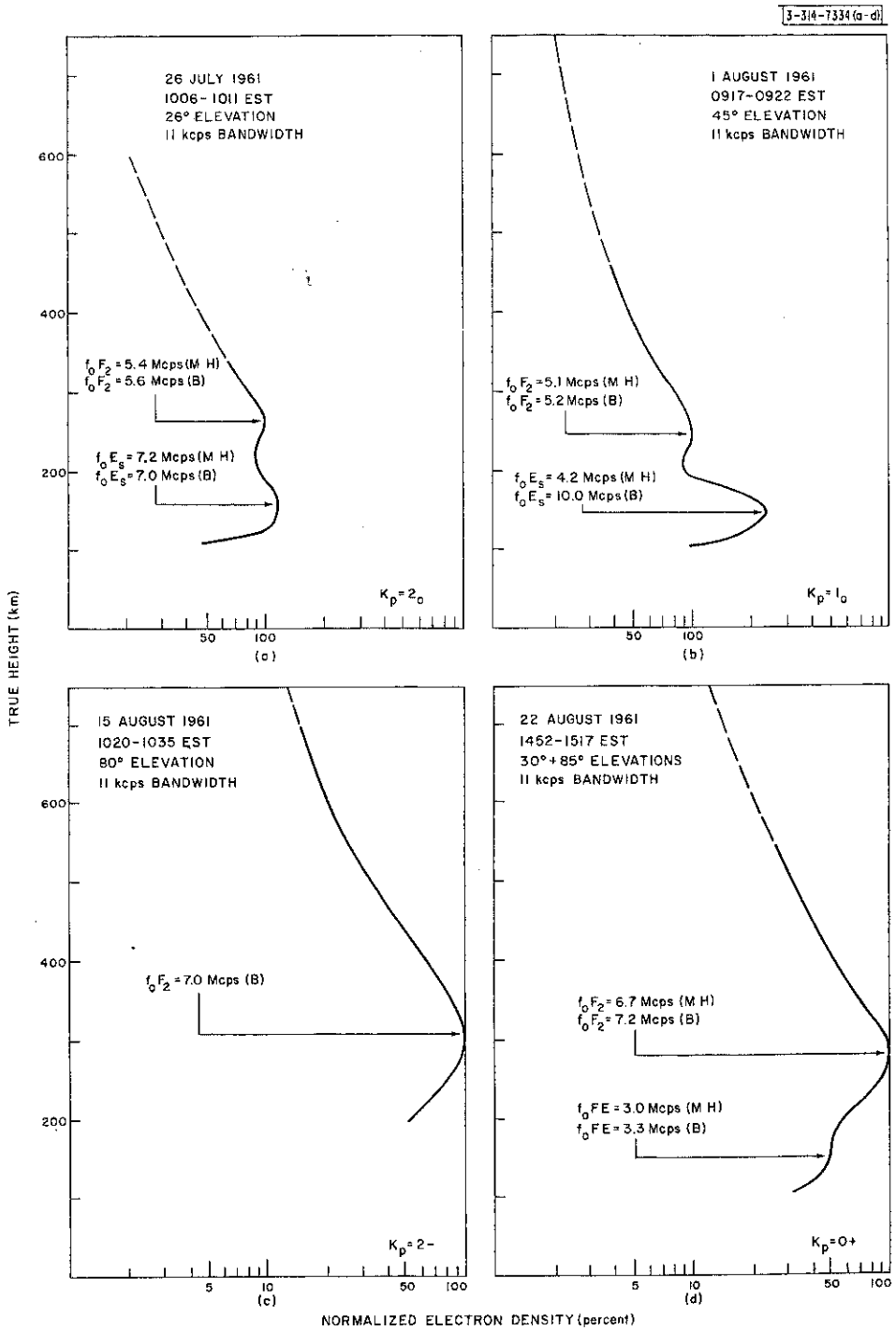

Fig. 12(a-d). Electron density profiles observed by means of the incoherent backscatter technique at Millstone Radar.

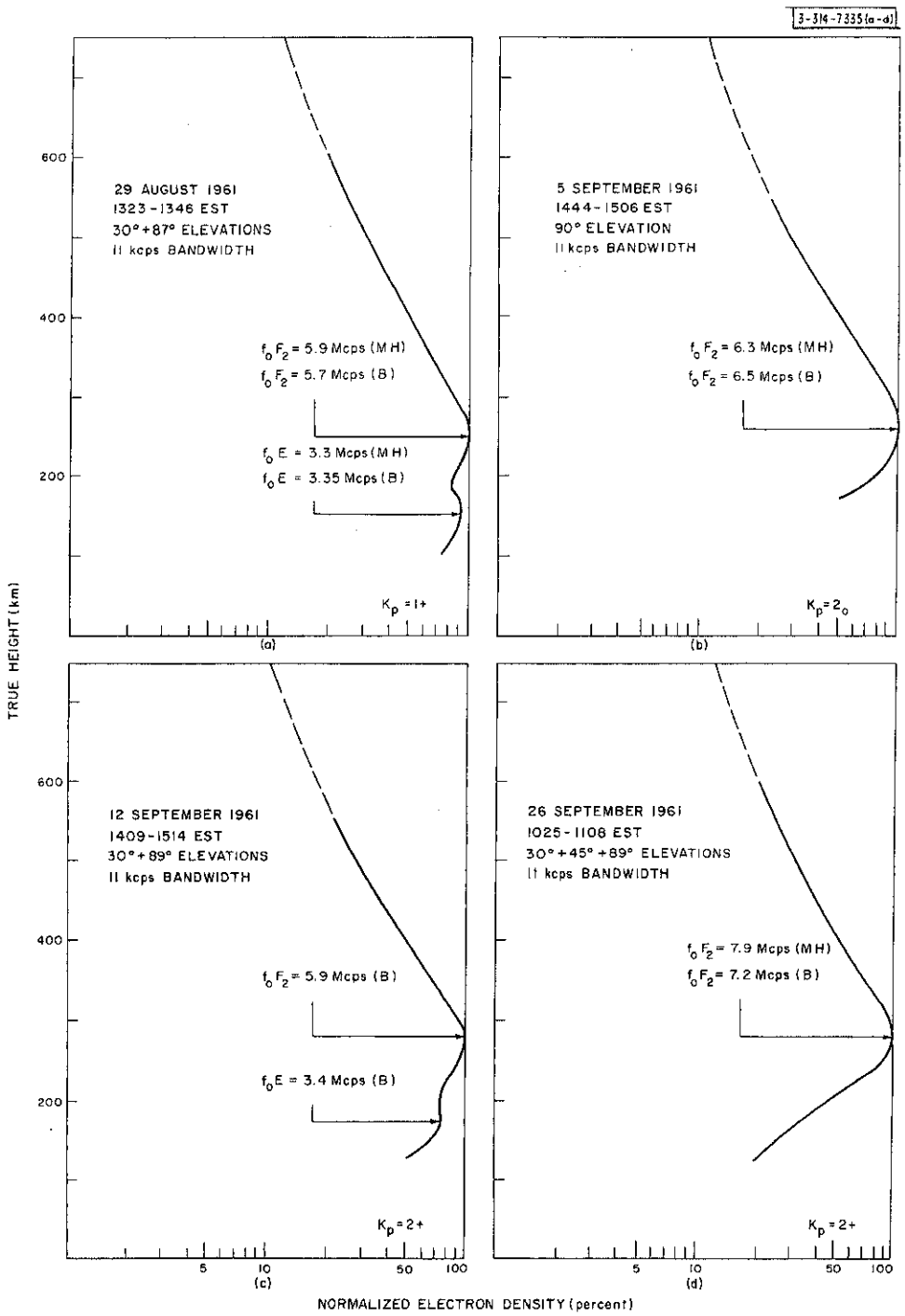

Fig. 13(a-d). Electron density profiles observed by means of the incoherent backscatter technique at Millstone Radar.

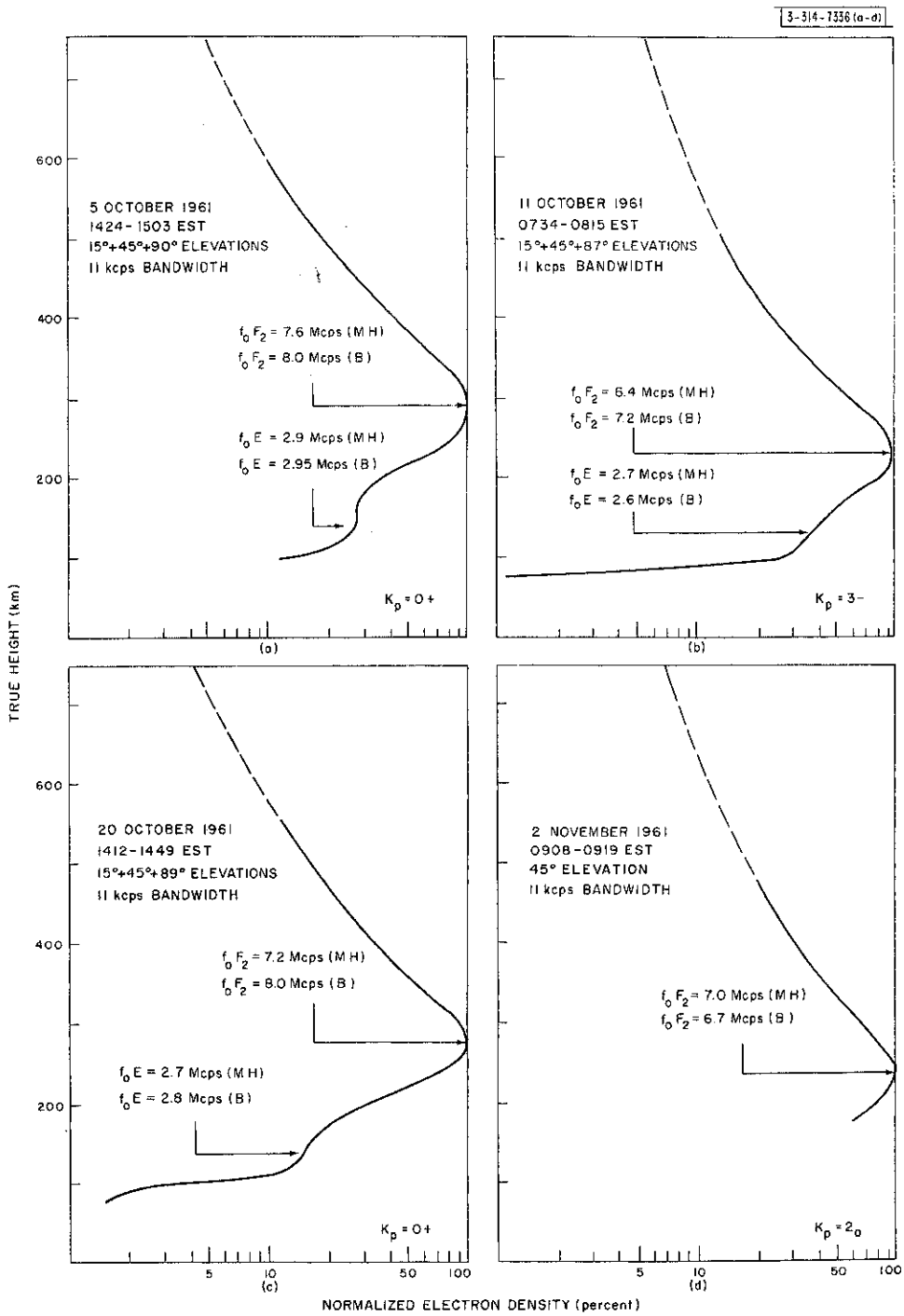

Fig. 14(a-d). Electron density profiles observed by means of the incoherent backscatter technique at Millstone Radar.

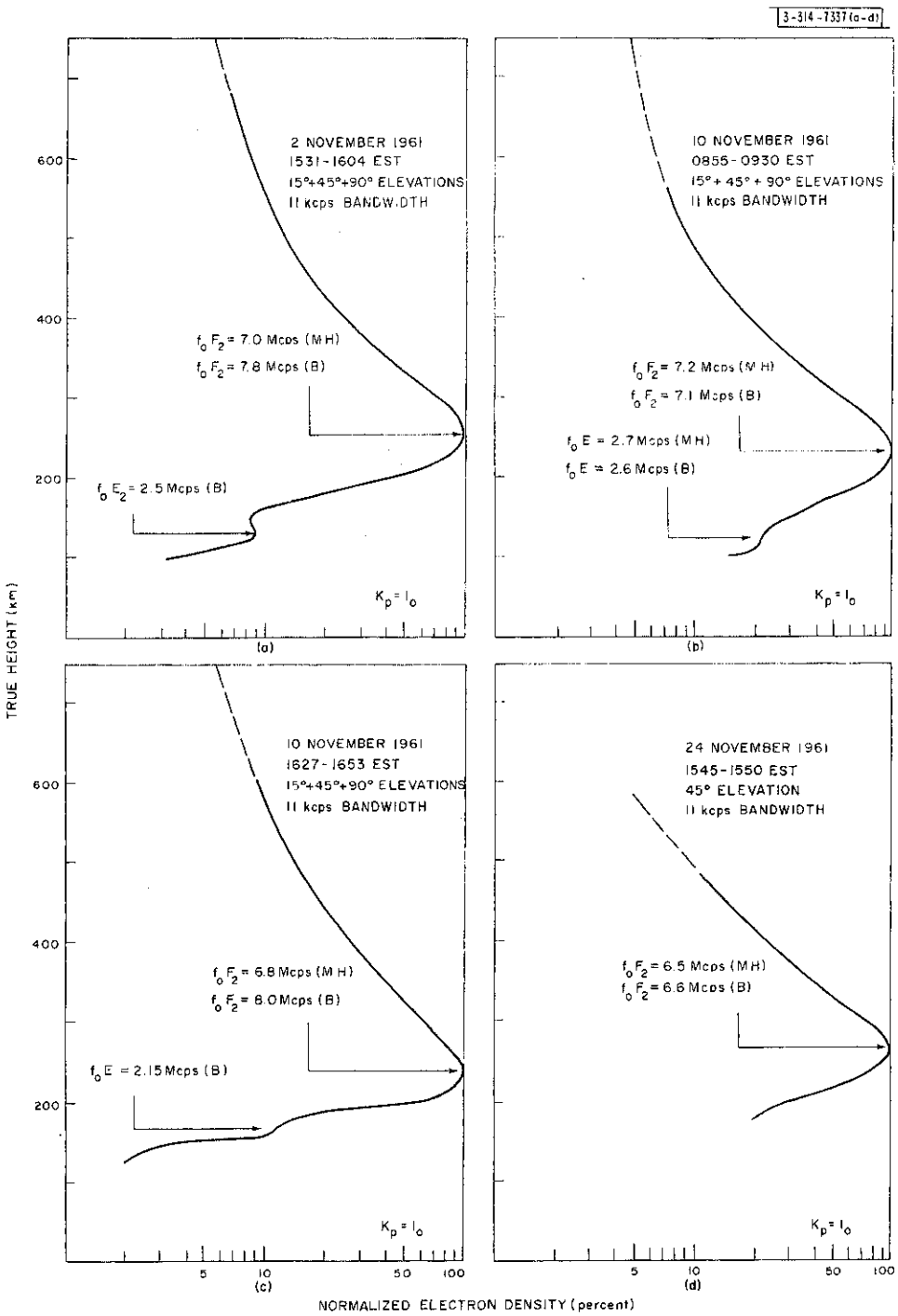

Fig. 15(a-d). Electron density profiles observed by means of the incoherent backscatter technique at Millstone Radar.

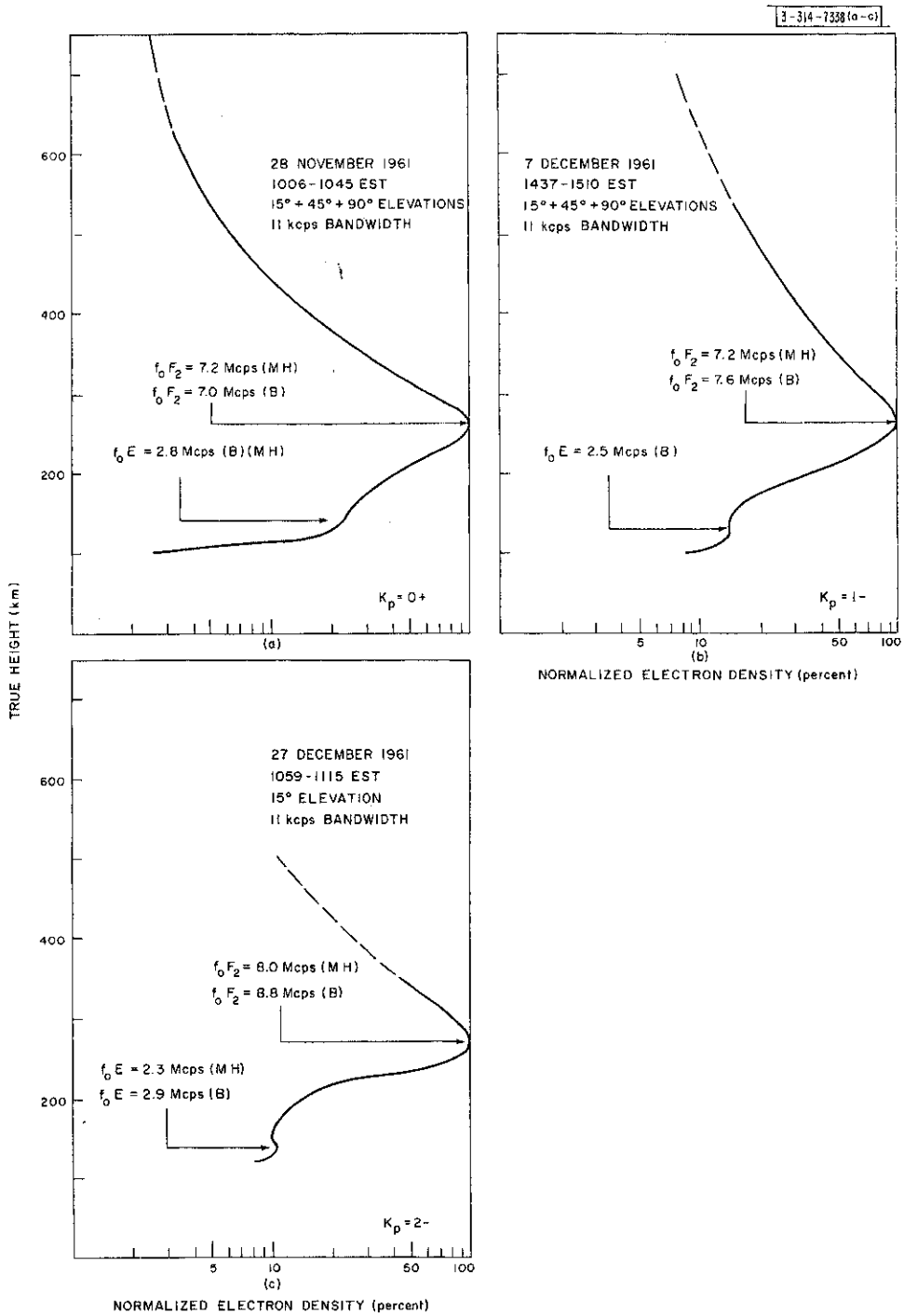

Fig. 16(a-c). Electron density profiles observed by means of the incoherent backscatter technique at Millstone Radar.

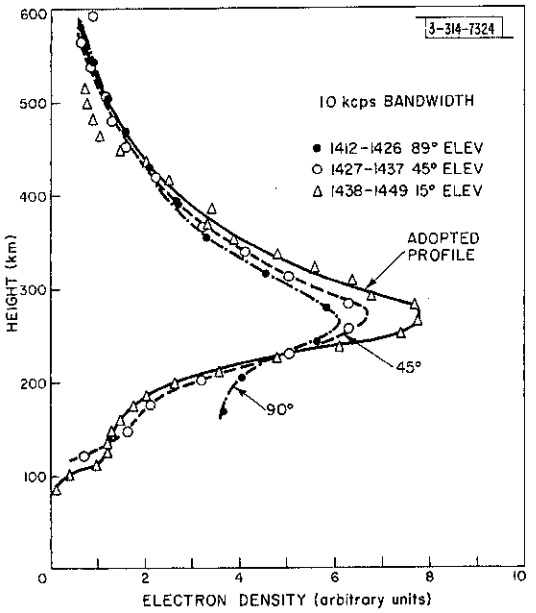

Fig. 17. The electron density profiles observed on 20 October 1961, when a 500-μsec transmitter pulse was employed and observations were made at the three antenna elevations designated.

over which the backscatter observations were made. They should represent the conditions in the ionosphere along the ray path fairly well, since the antenna was directed at an azimuth of 220° (corresponding to the bearing of Ft. Belvoir) when low elevation measurements were made. Early in 1961 a C-4 ionosonde was put into operation at Millstone Hill and additional values for the critical frequencies were obtained. These are indicated in the diagrams by "MH" in parentheses. In general, the values obtained at Millstone Hill and Ft. Belvoir are in good agreement, and where they differ a simple mean of the two values seems appropriate.

The only additional piece of information contained in each diagram (Figs. 3 through 16) is the value for the planetary magnetic index K_p. These values were obtained from the geophysical data presented in the Journal of Geophysical Research.

C. Accuracy of the Results

The undesirable effect of the convolution of the long (500-μsec) pulse used in these measurements with the true distribution of electrons has been mentioned earlier. For an elevation of 90°, the pulse occupies a height interval of 75 km; at 45° elevation it occupies 52 km, and at 15° elevation only 26 km. The receiver output is sampled at half these intervals. The finite bandwidth of the receiver (11 kcps) would have negligible effect until pulses as short as 100 μsec were employed. Errors due to this convolution exist in the shape of the profiles, as the progressive trend of the curves obtained at the three elevations shows in Fig. 17. An additional source of error is the somewhat arbitrary method of drawing a final curve through these points. Clearly, the profiles are not free of systematic errors, but it is difficult to estimate their magnitude.

The best method of checking the results is to compare them with other electron density measurements of the F-region. Bowles[5] and Millman, et al.,[20] have compared their backscatter observations with density profiles (up to the F2 maximum) obtained from the reduction of ionospheric soundings and found good agreement. However, in view of the discrepancies observed by Nisbet[21,22] between rocket profiles and ionosonde results, perphaps this is not the best of tests. In Figs. 18 through 20 the most accurate available rocket profiles[23-26] have been compared with the backscatter profiles which correspond most closely in time of day and year.

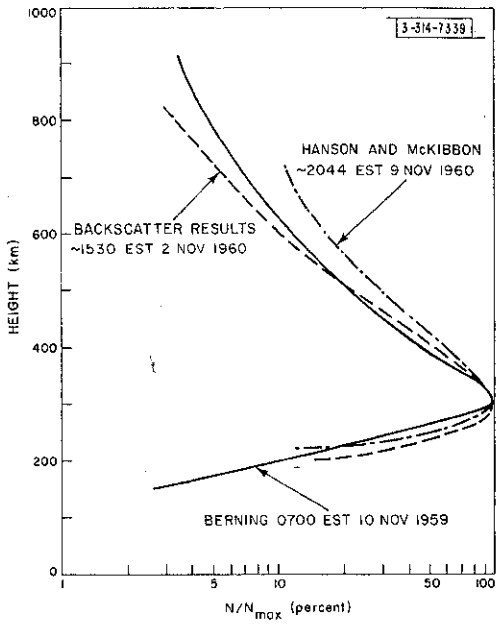

Fig. 18. The results of a single backscatter run during November 1960 compared with the results of rocket soundings from Wallops Island, Virginia, in November 1959 (Berning[24]) and November 1960 (Hanson and McKibbin[23]).

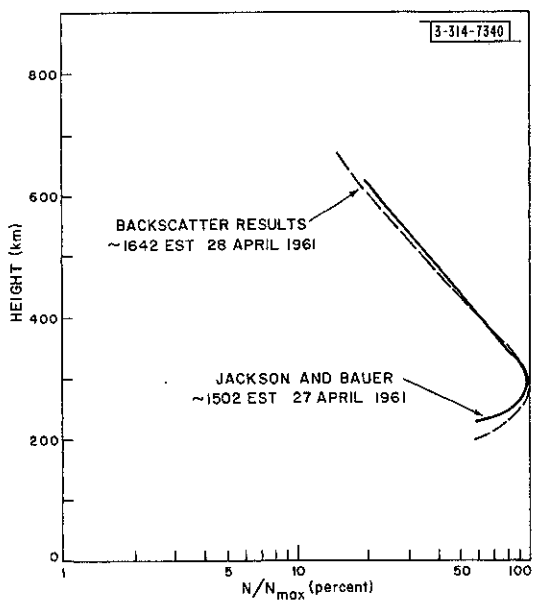

Fig. 19. The results of a backscatter run in April 1961 compared with the profile obtained from a rocket sounding from Wallops Island, Virginia, on the previous day (Jackson and Bauer[26]).

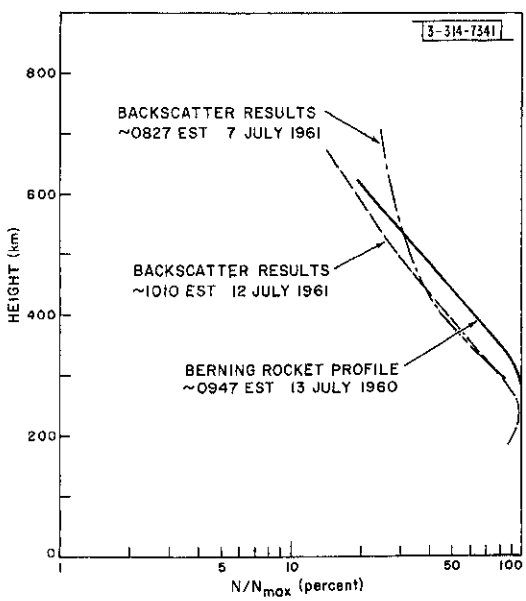

Fig. 20. The results of two backscatter profiles for July 1961 compared with a rocket profile obtained by Berning[25] in the same month a year before.

Unfortunately, in two cases backscatter results which could be compared with rocket data were not obtained in the same year; hence, rocket data taken one year have been compared (in these two instances) with backscatter profiles obtained a year later. We should not, therefore, expect good agreement in every case, but the degree of similarity observed between the backscatter and rocket profiles is sufficient to suggest that neither method is subject to large systematic error.

TABLE II

RATIO OF F_2 ELECTRON DENSITY N_{F2} TO THE E-REGION DENSITY N_E

Date	N_{F2}/N_E from Ionosonde Data	N_{F2}/N_E from Backscatter Data	Lowest Antenna Elevation
19 Mar 60	10.0	10.7	15°
2 Mar 61	6.5	2.6	45°
15 Mar 61	9.0	4.0	45°
24 Mar 61	7.3	3.8	90°
28 Mar 61	7.3	4.4	20°
5 Apr 61	4.8	1.8	20°
22 Aug 61	4.5	2.0	30°
29 Aug 61	3.2	1.1	30°
12 Sept 61	3.0	1.33	30°
5 Oct 61	6.9	3.6	15°
11 Oct 61	5.6	3.0	15°
20 Oct 61	7.1	6.6	15°
2 Nov 61	9.7	11.1	15°
10 Nov 61	7.1	4.2	15°
10 Nov 61	13.8	9.0	15°
28 Nov 61	6.25	4.2	15°
7 Dec 61	9.0	7.1	15°
27 Dec 61	11.6	9.0	15°

Another test which can be applied to these results is to examine them for internal consistency. For instance, one can check the ratio of the electron densities at the peak of the E- and F2-layers against those inferred from their critical frequencies. If the records that exhibit a sporadic E-echo are ignored, there are eighteen others that show both F2- and E-regions. These records are listed in Table II, which gives the ratio of the F2-electron density N_{F2} to the E-region density N_E expected from the ionosonde data and also to that actually observed. In five instances the observed and expected ratios agree to within ±20 percent. All these records were obtained when a lowest antenna elevation of 15° had been employed. In the remainder of the records, the expected ratio was on the average about twice that actually observed. There are four possible causes for this discrepancy:

(1) The F2 peak, being sharper than the ledge caused by the E-region, may suffer more because of the convolving effect of the long pulse.

(2) For elevations above 20°, weak ground clutter echoes may be present in the same range as the E-region echo, thereby yielding an unexpectedly high value of N_E.

(3) The presence of sporadic E ionization may be responsible for weak coherent echoes which also increase the observed value for N_E.

(4) The scattering cross section of the electrons is a function of the ratio between the electron and ion temperatures[27] and, therefore, decreases with altitude (Sec. III).

D. Discussion of the Results

1. General Considerations

Several interesting features of these profiles deserve comment. The E-region appears as a ledge in the ionization profile and does not usually exhibit a separate maximum. This may be caused in part by the inability of the measurements to resolve details smaller than about 20 km in height. No F1-ledge is observable in any profile, although it is present on ionosonde records during the daytime in summer at these latitudes. We conclude that the resolution was insufficient to permit its detection, and hence that this ledge occupies only a small height interval, approximately 10 to 20 km.

The presence of E_s can cause very strong returns (e.g., on 30 June 1961, 26 July 1961 and 1 August 1961). In the case of the profile observed on 1 August 1961, the E_s echo indicated a peak electron density of some 2.4 times that of the F2-region. The sporadic E-layer is always presumed to be thin (~1 km) because it is usually transparent to ionosonde echoes from the F-region. The elevation of the antenna employed on 1 August was 45°, so that the pulse would occupy a height interval of 52 km. We might expect, therefore, that the E_s-echo would be reduced (relative to the F-region echo) by a factor of 50, because of the ratio of the E_s-layer thickness to that of the pulse. The ratio of the electron density in the E_s-layer and the F2-region on this day appeared to be somewhere between 1:1 and 4:1 depending upon whether the Millstone Hill or the Ft. Belvoir ionosonde data is taken as most appropriate. Thus, we should not expect to see an observed ratio of 2.4:1 for the densities if the E_s-layer is thin. We are able to resolve the paradox by assuming either that the E_s-layer is as thick as the pulse (~50 km), or that irregular regions of electron density, large compared with the wavelength, existed which yielded semi-coherent echoes. These regions need not be critically dense, but might scatter like auroral ionization.[28] This latter explanation seems the more acceptable and supports the view that sporadic E-echoes are caused by irregular, dense regions of ionization. When present only in a weak form, these irregularities may contribute to the unexpectedly high values of E-region electron density discussed previously.

Spread-F echoes were frequently observed on ionosonde records, particularly during the early morning hours, but no F-region echoes of unusually high intensity were observed in the backscattered signals. Thus, it seems that the resolution (both in time as well as height) available for these measurements was insufficient to detect a spread-F condition, and that the irregularities in the electron density which are responsible for spread F are not as great as those observed in sporadic E.

In view of the above comments, it seems unwise to place a great deal of reliance on the electron density profiles below about 200 km. When better equipment becomes available, the backscatter method may be able to challenge the ionosonde in this region, but at the present time its value lies largely in the ability to obtain the electron density distribution above N_{max}. It is with this feature that the remaining discussion will be concerned.

2. The Height of Maximum Electron Density h_{max}

There are insufficient profiles to permit a detailed examination of the diurnal variation of the profile shape (although Pineo and Hynek[29] have attempted this for one day in May 1961). Instead, only the variation of h_{max} and the scale height H_i of the ionization above h_{max} will be investigated.

The values for h_{max} observed in summer and winter (taken as the time between equinoxes) are shown in Figs. 21(a-b). During both seasons there seems to be a tendency for h_{max} to increase throughout the day. The actual values are about what might be expected from the table published by Brice[30] if allowance is made for the fact that the measurements were made approximately midway between sunspot maximum and minimum.

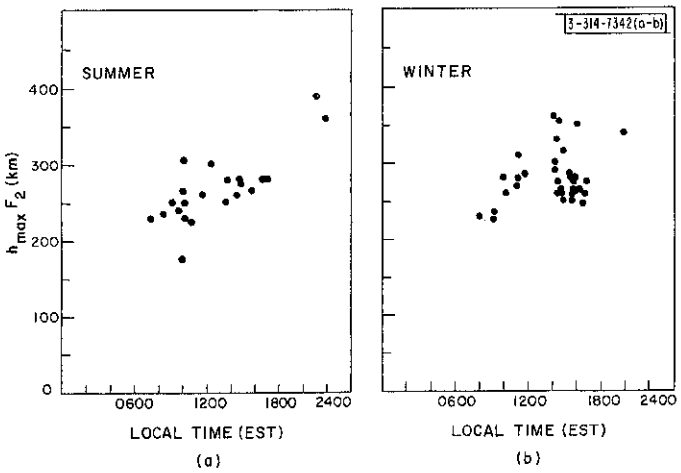

Fig. 21(a-b). Values for the height of maximum density h_{max} observed in (a) summer and (b) winter (taken from the curves presented in Figs. 4 through 17).

3. Scale Height H_i above h_{max}

Some comparisons of the profiles are provided in Figs. 22 to 24. In Fig. 22, ten winter day profiles obtained in 1960 have been plotted together, after adjusting their actual heights to their mean height (280 km). These profiles were selected from the data because f_oF2 was 10 ± 1 Mcps in every case, and the average critical frequency was 10 Mcps. Also shown in Fig. 22 is a set of points representing a Chapman[31] region computed for a scale height H of 50 km and a solar zenith distance χ of 60°. As noted in the previous review,[16] the electron density in a Chapman region diminishes as $\exp\{(1/2)[1 - z - (\exp -z) \sec\chi]\}$ where z is the height in units of one scale height H. For values of zenith distance χ of 60° or less and $z \geq 3$, the term $(\exp -z) \cdot \sec\chi$ can be neglected, and the density decreases with an apparent scale height that is twice the scale height of the neutral particles. Thus, Fig. 22 indicates that over the height range 300 to 500 km the scale height of the ionization H_i is of the order of 100 km, but gradually increases above this level. In Figs. 23 and 24, some summer profiles have been superimposed. For this purpose, the division between summer and winter was taken simply as the time between the equinoxes, since insufficient profiles were available to divide the year into four seasons. Figure 23 shows five morning profiles, and Fig. 24 shows five taken in the afternoon. All ten were selected because $f_oF2 = 6.5 \pm 1$ Mcps. The mean critical frequency and the mean height to which individual profiles have been adjusted are stated. In the morning a Chapman region where H ~ 65 km (χ = 30°) provides an approximate fit to the results, and in the afternoon H ≈ 70 km (χ = 30°) provides a reasonable fit.

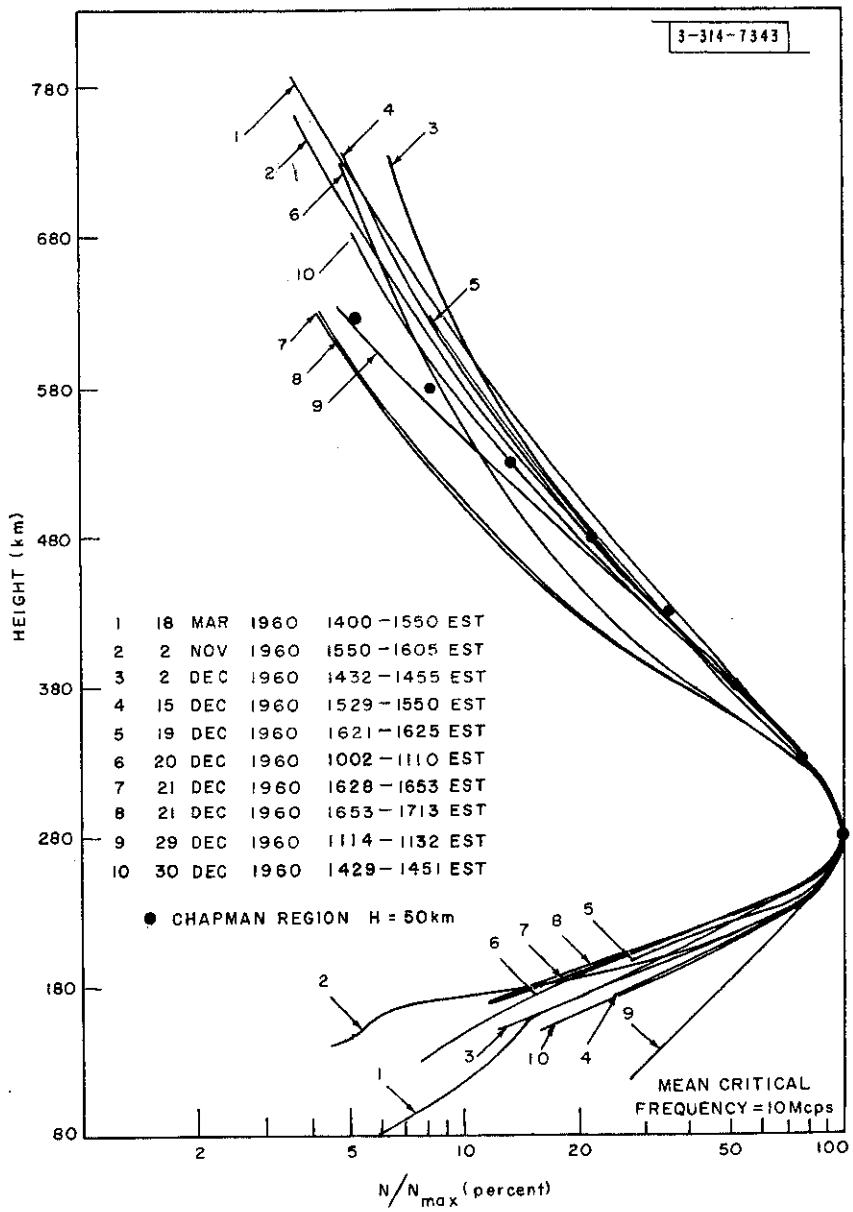

Fig. 22. Ten winter profiles observed in 1960 are superimposed. The true heights have been adjusted so that each curve reaches a maximum at the mean value for h_{max}.

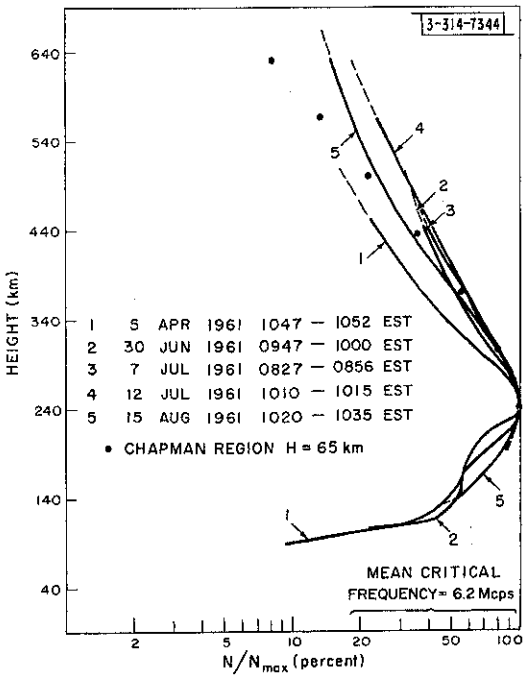

Fig. 23. Five summer morning profiles observed in 1961 are superimposed. The true heights have been adjusted so that each curve reaches a maximum at the mean value for h_{max}.

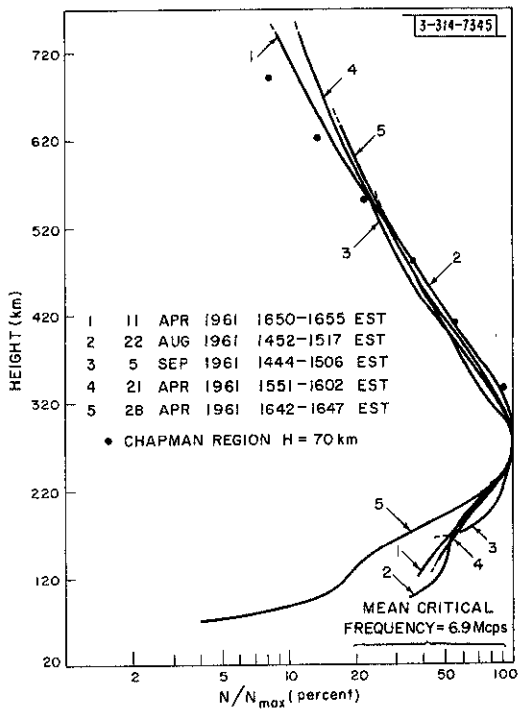

Fig. 24. Five summer afternoon profiles observed in 1961 are superimposed. The true heights have been adjusted so that each curve reaches a maximum at the mean value for h_{max}.

Mean values for the scale height H_i of the ionization above N_{max} have been obtained in the following way. The gradient on each profile was estimated at height intervals of 100, 150, 200 and 250 ... km above the observed level of N_{max}. The profiles were divided into summer and winter, and the day subdivided into three roughly equal intervals. The mean values for H_i obtained in this way are shown in Figs. 25 and 26, together with the estimated error ΔH_i computed by simply assuming that the observed spread of values represents statistical variations due to random errors of measurement. In every case H_i is found to increase with height. These results are summarized in Table III. The data points used in Figs. 25 and 26 were later replotted as a function of their true height. Figure 27 provides a representative example of one of these diagrams. A least-mean-square linear relation was next obtained for each diagram, and the results of this analysis are presented in Table IV.

Some of the differences between Tables III and IV relate to the different methods of averaging the results. However, certain trends are clearly visible in both tables. These are:

(a) In winter there is little diurnal variation in either the value of H_i at a given height or the slope dH_i/dh.

(b) In summer there is a marked increase in H_i and dH_i/dh following sunrise and a decline in both these quantities throughout the day.

(c) The summer values of H_i averaged over the whole day are higher than those observed in winter.

Several authors[32,33] have postulated that electron density in the upper part of the F-region is not governed by the competing processes of production and recombination, but by mass motions. They show that the ions, in attempting to seek a hydrostatic equilibrium condition under the influence of gravity, tend to move downward, bringing the electrons with them due to coulomb

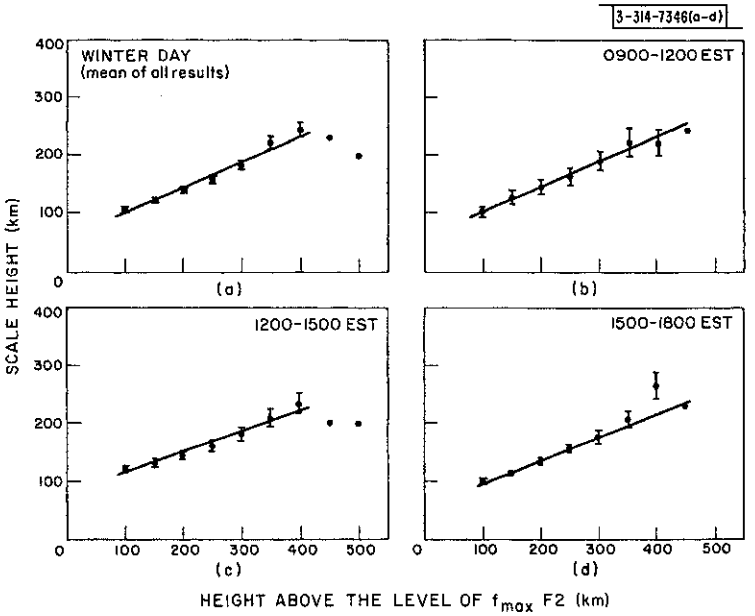

Fig. 25(a-d). The mean value of the scale height H_i observed at different distances above h_{max} for (a) the whole day, (b) 0900 – 1200 EST, (c) 1200 – 1500 EST, (d) 1500 – 1800 EST in winter.

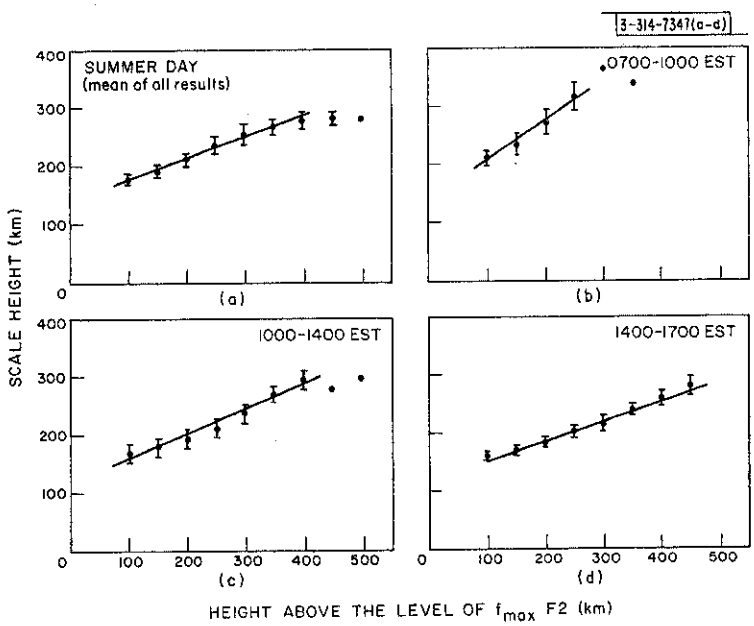

Fig. 26(a-d). The mean value of the scale height H_i observed at various distances above h_{max} during the time indicated (all taken in summer).

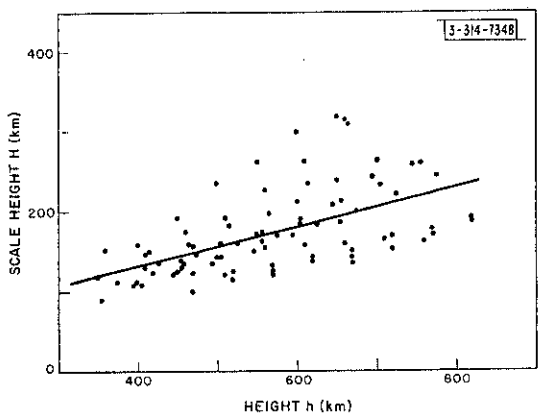

Fig. 27. The values for scale height H_i plotted as a function of true height h for the winter day period 1200 – 1500 EST. The straight line is a least-mean-square fit to the points.

TABLE III

THE MEAN VARIATION OF THE SCALE HEIGHT H_i WITH HEIGHT ABOVE THE LEVEL OF N_{max} ($h-h_{max}$) FOR SUMMER AND WINTER BACKSCATTER OBSERVATIONS, 1960-61

Winter				Summer			
Period	H_i at $h-h_{max} = 250$ (km)	ΔH_i	$\frac{dH_i}{d(h-h_{max})}$	Period	H_i at $h-h_{max} = 250$ (km)	ΔH_i	$\frac{dH_i}{d(h-h_{max})}$
All day	170	±7	0.40	All day	232	±14	0.36
09 – 12	167	±14	0.43	07 – 10	309	±23	0.68
12 – 15	170	±8	0.35	10 – 14	223	±15	0.43
15 – 18	155	±6	0.40	14 – 17	200	±10	0.57

TABLE IV

THE MEAN VARIATION OF SCALE HEIGHT H_i WITH TRUE HEIGHT h FOR SUMMER AND WINTER BACKSCATTER OBSERVATIONS, 1960-61

Winter				Summer			
Period	h_{max} (km)	H_i at h = 500 (km)	dH_i/dh	Period	h_{max} (km)	H_i at h = 500 (km)	dH_i/dh
All day		157	0.32	All day		224	0.26
09 – 12	270.5	158	0.25	07 – 10	230.0	304	0.56
12 – 15	297.9	156	0.25	10 – 14	268.8	211	0.42
15 – 18	272.8	152	0.30	14 – 17	273.1	197	0.29
				Night	~380	132	0.28

attraction. Since the electrons are considerably lighter, and would in the absence of the ions form their own equilibrium distribution with a much larger scale height, their presence modifies the distribution achieved by the ions. The net result is that the scale height of the ionization H_i is given by

$$H_i = \frac{k(T_e + T_i)}{m_i g} \quad , \tag{3}$$

where

T_e = electron temperature ,

T_i = ion temperature ,

m_i = ionic mass ,

g = acceleration due to gravity .

Bauer and Jackson[26] have argued that the rocket results can be interpreted as indicating that ion diffusion is the controlling factor in this region, and that $(T_e + T_i)$ equals a constant. An isothermal region above about 300 km was postulated by Nicolet[34] on theoretical grounds concerning the conductivity in this region, and a constant temperature for this region has been assumed in the atmospheric model published by Johnson.[35] However, the author[16] has pointed out that (a) as Fig. 18 shows, not all the rocket profiles indicate a constant scale height H_i, (b) sometimes the backscatter profiles indicate an almost constant value for H_i, but more often they do not, and (c) the scale height observed for the neutral particles H_N from satellite drag observations[36-41] all tend to increase with height. In Fig. 28, values for the scale height of the neutral particles

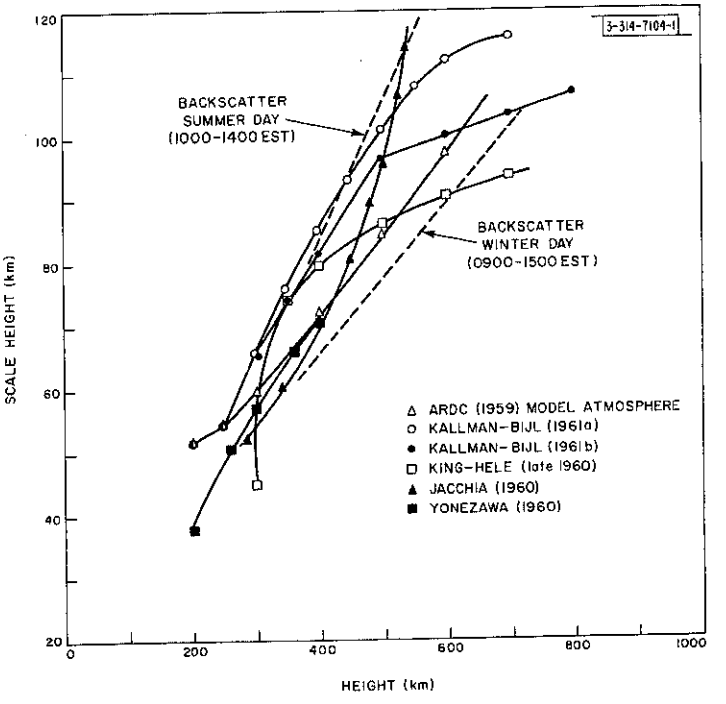

Fig. 28. The midday summer and winter values for the scale height of the neutral particles H_N obtained from the backscatter values of H_i by assuming $H_N = H_i/2$, together with satellite drag values for H_N according to various authors.[36-41]

TABLE V

THE RATIO OF THE NUMBER OF ELECTRONS n_a ABOVE N_{max} TO THE NUMBER BELOW n_b

(Winter Day Observations)

Date (1960)	Time (EST)	Ratio $n_a:n_b$
18 Mar	1400 – 1550	1.93
2 Nov	1550 – 1605	2.30
2 Dec	1422 – 1455	2.20
15 Dec	1529 – 1550	1.90
19 Dec	1621 – 1625	1.97
20 Dec	1002 – 1110	1.64
21 Dec	1628 – 1653	2.05
21 Dec	1653 – 1713	2.06
29 Dec	1114 – 1132	1.32
30 Dec	1429 – 1451	1.91
Mean = 1.93 ± 0.26		

obtained by various authors are compared with the scale height of the ionizable constituent obtained from the backscatter results by using Eq. (3) and assuming $T_e = T_i$. That is, the scale height of the ionizable constituent has been assumed to be half that of the ionization H_i. It can be seen that the summer and winter curves bracket most of the other observations.

4. The Total Electron Content of the Ionosphere

Values for the total electron content of the ionosphere have been obtained by several workers using a variety of techniques. From their measurements values have been obtained for the ratio between the number of electrons n_a above N_{max} to the number below n_b. The most recently published values for this ratio were obtained at Jodrell Bank during the winter of 1959,[42] by means of the moon-echo technique. These results yielded an average daytime ratio of about 3:1. The winter profiles shown in Fig. 22 were used for comparison and the values listed in Table V for $n_a:n_b$ were obtained. These values were obtained by plotting the density as a linear function of height and extrapolating the profile both above and below N_{max}. Below N_{max}, the small amount of necessary extrapolation can be performed with a fair degree of confidence by following the curve of Fig. 4(b) obtained on 18 March. Above N_{max}, the electron density was extrapolated to 800 km, beyond which it was assumed to decay with a constant scale height of H_i = 150 km. The ionization above 800 km constituted about 10 percent of n_a.

The mean value of the ratio $n_a:n_b$ obtained in this way is about 2 to 1, which is significantly lower than that obtained at Jodrell Bank. It is possible that the moon-echo result is too high because n_b, when obtained from ionosonde data, is too low.[21,22] However, Seddon[43] doubts this explanation since his studies indicate good agreement between rocket and ionosonde measurements. Taylor[44] has suggested that the oblique path of the rays through the ionosphere in the moon-echo work may introduce erroneous values in the ratio $n_a:n_b$ if there are marked variations in the electron content as a function of latitude. Millman and Rose[45] have reported measurements of $n_a:n_b$ at Trinidad (11°N) and found daytime ratios lying between 1:1 and 2:1. It seems

probable, therefore, that this ratio may be a function of latitude, so that a comparison of the results obtained at Millstone (42°N) with those at Jodrell Bank (54°N) or Trinidad (11°N) would be improper.

III. SPECTRUM MEASUREMENTS

A. Introduction

A measurement of the spectral distribution of the energy in the reflected signal contains at least as much information as a measurement of the electron density profile. This is true because the shape of the spectrum depends upon the ratio of electron temperature to ion temperature, $T_e:T_i$. This dependence is shown in Fig. 29, where curves obtained by Fejer[6] for the distribution

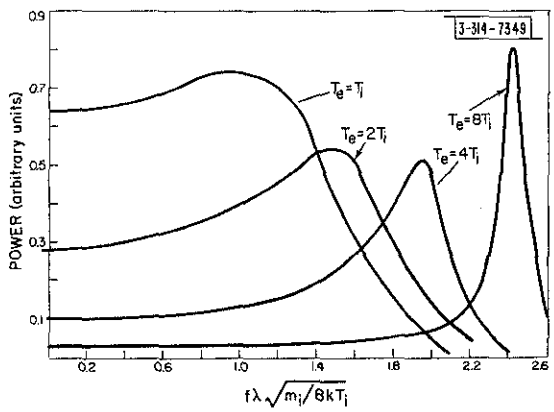

Fig. 29. The theoretical power spectra computed by Fejer[6] for different values of the ratio between the electron and ion temperatures $T_e:T_i$.

of echo power with frequency for different ratios $T_e:T_i$ are reproduced. It should be made clear that the spectra are double-sided with only one half shown in Fig. 29. This figure is valid for the case where the radio wavelength λ is considerably greater than the Debye length λ_D [Eq. (2)], and therefore is applicable to the results reported in this paper. The abscissa in Fig. 29 is the Doppler shift f normalized by multiplying by the radio wavelength λ and a term related to the velocity of sound for the ions where m_i equals mass of the ions, k equals Boltzmann's constant and T_i equals ion temperature. Other assumptions used in the derivation of Fig. 29 are (a) all the atoms are singly charged, (b) only one type of ion is present, (c) collisions are infrequent and may be neglected and (d) the ray path is not inclined at an angle to the magnetic field lines $\geqslant 85°$.

Several authors[7,9,11] have investigated magnetic field effects, i.e., the removal of restriction (d), and Pineo and Hynek[46] have reported an experimental investigation of these effects. Pineo and Hynek found good qualitative agreement between their results and theoretical spectra computed by Renau, Camnitz and Flood[47] for different inclinations between the ray path and the field lines. In order to perform this investigation, Pineo and Hynek were compelled to make use of a high-power radar system on Trinidad. It is not possible by use of the Millstone Hill radar to achieve a ray path at right angles to the magnetic field lines above a height of 100 km (in the F-region). Hence, for any measurements made here, restriction (d) is observed. Fejer[6] has considered the effect of the removal of restriction (b) and presented curves showing the spectra for different mixtures of oxygen and helium atoms. This choice was presumably dictated by the current view that at most F-region heights O^+ is the principal ion. The theoretical arguments for this viewpoint have been summarized by Rishbeth,[48] and satellite-borne mass-spectrometer measurements which confirm this result have been reported by Poloskov[49] and Istomin.[50]

Nicolet[51] has argued that the outermost part of the earth's atmosphere (beyond approximately 1000 km altitude) consists of a helium layer, and Bauer,[52] and Bauer and Jackson[53] present evidence in the form of an electron density profile to 1600 km (obtained by a rocket fired from Wallops Island, Virginia) which supports this view. With the present equipment, spectrum measurements can be obtained only up to a height of approximately 600 km, where the expected number of helium ions would be insufficient to influence the spectral shape. For these observations, therefore, we should expect, on the basis of the available evidence, that condition (b) will be fulfilled, and that the mass of the ion m_i will be that of oxygen ($m_i = 2.675 \times 10^{-23}$ grams). It follows that the width of the spectrum may be used to determine T_i.

Ratcliffe and Weekes[54] suggest that at F-region heights the collision frequency of the electrons is approximately 1 kcps (most collisions being with other charged particles). Since this frequency is so low compared to the radio frequency, it is appropriate to assume that condition (c) will be fulfilled. The presence of doubly or triply charged ions remains an open question at the present time. However, since the number of neutral particles exceeds the number of charged particles at most F-region heights by two or more orders of magnitude, we might expect singly charged atoms to predominate by a large margin.

Spectral measurements of the signals observed at Millstone Hill have been reported by Pineo, et al.[13,15,29]. Pineo and Hynek[29] conclude from the shape of the spectra that over most parts of the day $T_e \sim 2T_i$, but at night $T_e \sim T_i$. The nonequilibrium condition of the electron and ion temperatures in the daytime is supported by the rocket measurements of Spencer, et al.[55] in which temperature could be inferred from the volt-ampere curves of a dumbbell probe. Also, Bowles[56] has reported that the electron cross section decreases around sunrise, which would indicate that, at least over this period, the equilibrium conditions are disturbed. This evidence is contrary to the generally accepted view that equilibrium between the electron and ion temperatures prevails throughout most parts of the ionosphere (Johnson[57]) and to the experimental measurements reported by Serbu, et al.[58] using Explorer VIII. Clearly, there is much to be gained by further spectrum measurements.

The method employed by Pineo and Hynek[29] was as follows. The normal receiver filter, nominally 11 kcps, is replaced by a narrow-band (800-cps) filter, and the integration process is performed repeatedly as this filter is tuned across the signal. The electron densities corresponding to a given height are then selected from each density profile and plotted as a function of the offset frequency of the filter to yield a spectrum. Usually about an hour's time is required to obtain a curve containing, say, 6 points. The method suffers from the obvious disadvantage that any changes of the electron density as a function of time will show up as a distortion of the spectrum obtained in this way. In order to overcome this problem, the author constructed a spectrum analyzer.

B. The New Spectrum Analyzer

The rebuilding of the Millstone Hill radar during 1962 provided an opportunity to acquire a large number of crystal filters. These filters have a response resembling that of a single-pole filter (i.e., approximately Gaussian) and a bandwidth between half-power points of 160 cps. The filters have center frequencies in the vicinity of 200 kcps, but are spaced at 160-cps intervals. The twenty-four filters selected spanned the range from 200 to 212 kcps at approximately 500-cps intervals and permitted the upper sideband of the reflected signals to be examined over a Doppler frequency range of 0 to 12 kcps. The filters are driven by a gated amplifier (Fig. 30), which selects

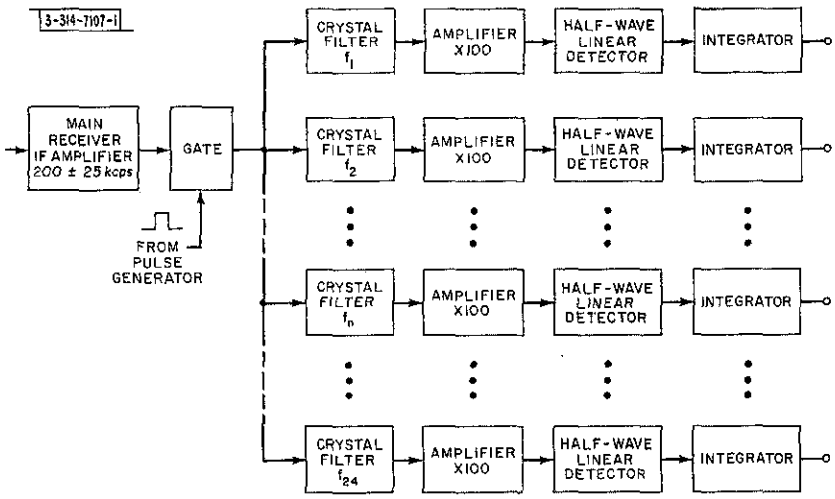

Fig. 30. Block diagram of the new spectral analyzer.

from the time base a region corresponding to a given height interval. Each filter is followed by an amplifier capable of delivering a ±100-volt peak signal to the detector. The detectors are silicon diodes in a simple half-wave circuit, which, when driven by these large signals, behave as almost identical linear detectors. (It was not considered feasible to make and match twenty-four square-law devices.) The currents from the detectors are summed by integrators (Fig. 30). Each integrator circuit consists of a chopper-stabilized DC amplifier (Philbrick USA 4JX) arranged in a Miller circuit with a self-time constant of several hours. During a 5-minute integration period the voltages build up to approximately 60 volts and far exceed the voltage introduced by drifts or DC offsets in the DC amplifiers (approximately 0.1 volt). No attempt was made to match the gains of each of the 24 channels. Instead, after each measurement of signal energy, the timing circuits were adjusted to place the gated portion of the time base at a range where no signal could be expected, and the measurements were repeated on background noise alone. Ratios are then taken of each of the two voltages, which are next squared to yield the signal-to-noise ratio at each frequency. The filters in the region 8 to 12 kcps sample only noise during either measurement, because at 440 Mcps the spectrum is only approximately ±6 kcps wide. It follows, therefore, that the mean of the ratios observed for these filters should be 1:1. If not, it can be presumed that the gain (or the ambient noise level) of the receiver ahead of the gated stage has changed between runs (the duration of each run is timed to within 1 msec). All the points may then be scaled by some constant factor to bring the mean ratio observed for the last 8 (or so) filters to unity. In this way a spectrum measurement containing 24 points is obtained in 5 or 10 minutes, which does not suffer from any of the ambiguities that arise from use of the earlier method. Unfortunately, the spectrum is measured only at a single height. In order to obtain spectra at a range of different heights, a period of approximately 1 hour is required during the day and approximately two hours at night when the signals are much weaker.

C. Results of Observations in 1962

On 4 days early in 1962 (15 to 16 February, 13 to 14 and 26 to 27 March and 1 to 2 April) observations were made over a complete 24-hour period. The inclusion of some of the results of these measurements in this report is warranted by their bearing on the interpretation of the results presented in Sec. II.

The compromise between range resolution and echo intensity discussed in Sec. II is further complicated during spectral measurements by the need for a long pulse in order to minimize the spectral width of the transmissions. For most measurements a pulse length of 1 msec was chosen. Such a pulse would add approximately 500 cps, or 10 percent, to the half-width of the signals, but for some measurements a pulse length of 2 msec combined with a very low elevation (9°) was used for better frequency resolution. In order to achieve a reasonable degree of range resolution, all measurements were made at elevation angles of 50° or less, in contrast to those of Pineo and Hynek,[29] who took the measurements in the zenith. A point was chosen on the surface of the earth in the vicinity of Washington, D.C., and all the measurements were made at ranges corresponding to different heights vertically above this point. This seemed to provide about the best compromise between range resolution, frequency resolution and signal intensity. Thus, in order to illuminate different height intervals, the antenna elevation was changed, and the gated portion of the time base was adjusted to an accuracy of ±5 μsec. Measurements were made at ranges corresponding to heights of 200, 300, 400, 500, 600 and 700 km, though on most days only 400 and 600 km or 500 and 700 km of the last four were examined. Because the signals are exceedingly weak at night, a 15-minute period of integration was employed for most observations. The complete sequence of heights could then be examined only once every 2 hours.

Figure 31 presents a series of spectra corresponding to a height of 300 km and obtained during the period 1 to 2 April. (The actual region illuminated by the pulse was from 265 to 335 km.)

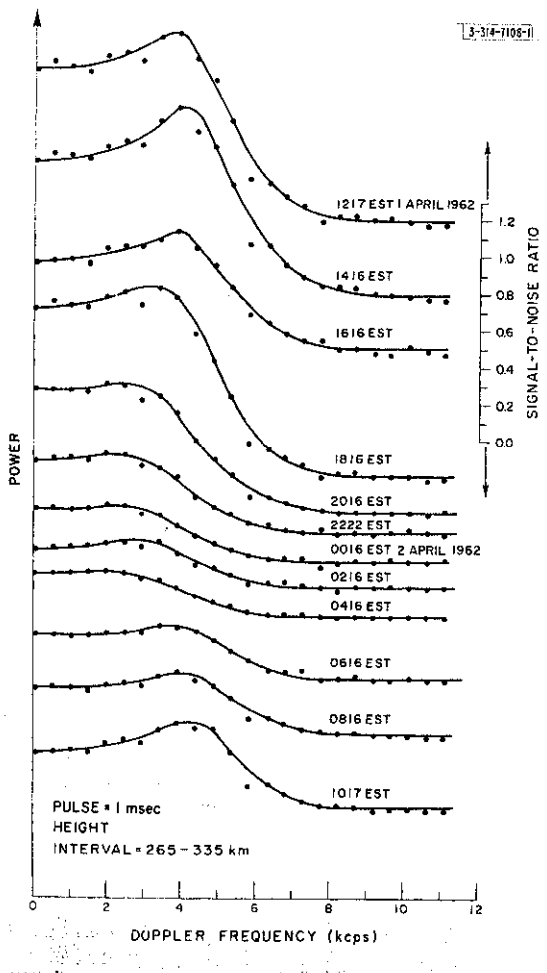

Fig. 31. Spectra obtained for incoherent backscatter signals at a delay corresponding to 300 km height, 1 to 2 April 1962.

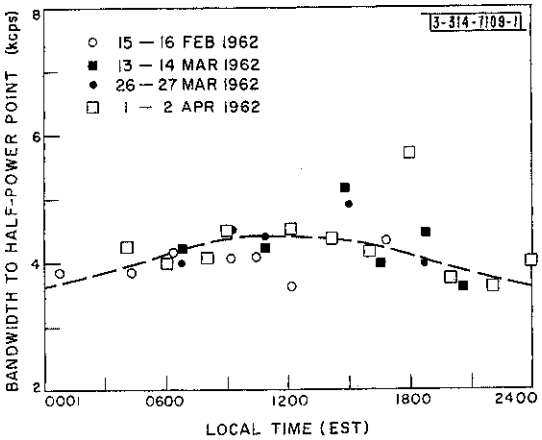

(a)

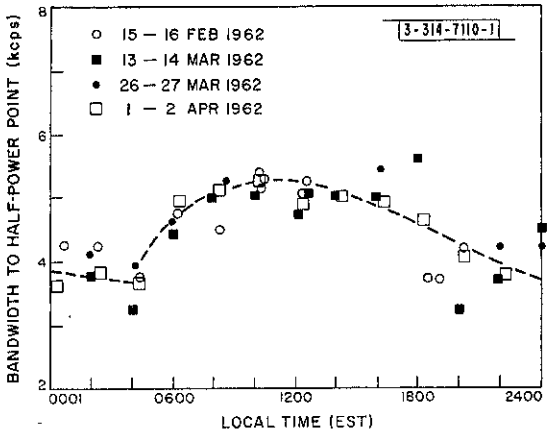

(b)

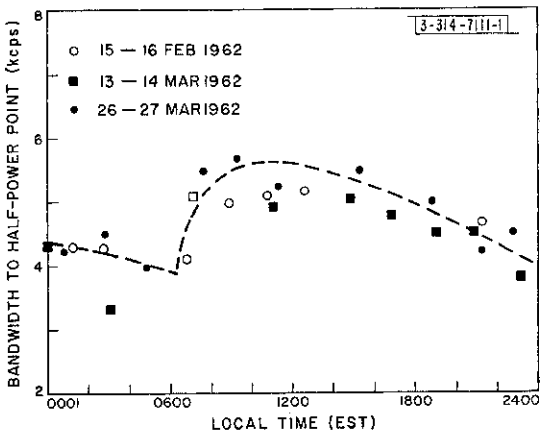

(c)

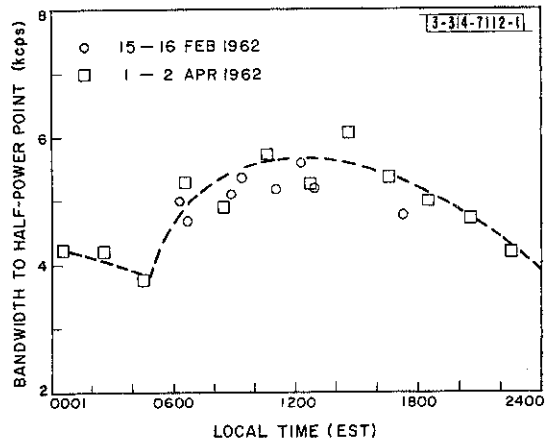

(d)

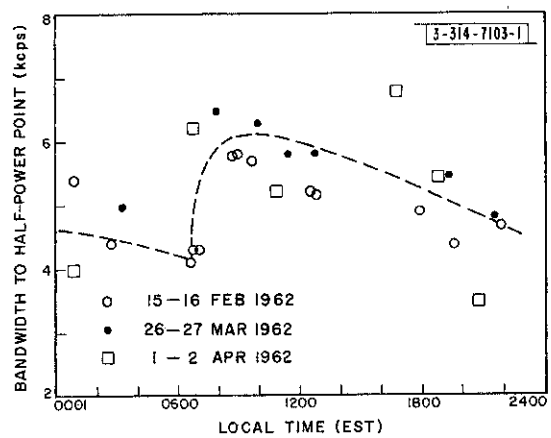

(e)

Fig. 32(a-e). The half-bandwidth of the signals observed at a delay corresponding to a height of (a) 200 km, (b) 300 km, (c) 400 km, (d) 500 km and (e) 600 and 700 km.

These results were obtained by using 1-msec transmitter pulses together with a 1-msec receiver gate width. Although the absolute signal-to-noise ratio is a function of the receiver noise figure and transmitter power – neither of which is wholly stable – there is a clear diurnal variation of the intensity of the signals. What is more important, there is also a clear diurnal variation of the spectral width of the signals, together with small changes in the spectrum shape.

The bandwidth of each of the spectra has been measured in the following way. The half-power point, taken as the frequency at which the power is half the value observed in the wing of the curve, is first extracted. These values are reduced by 500 cps for curves obtained using 1-msec pulses and 250 cps where 2-msec pulses were employed. These correction factors are not precise but serve to make a first-order correction for the increased width of the spectra because of the finite spectral width of the pulses. The values for the bandwidth obtained in this way at 200, 300, 400, 500, 600 and 700 km height are shown in Figs. 32(a-e), respectively. The values obtained at 600 and 700 km were few in number because of the poor quality of the results obtainable at these heights, and are presented together in Fig. 32(e). Some of the spectral measurements were spoiled by interference during either the signal or the noise calibration run. The average nighttime (2200-0300 EST) and daytime (0900-1500 EST) values for the bandwidth as a function of height are shown in Fig. 33. The vertical bars associated with the points in these curves represent the height interval occupied by the pulse, whereas the horizontal bars indicate the rms scatter of the values. It will be noted that above 300 km the bandwidth does not vary rapidly with height. This behavior is to be expected, since the bandwidth is proportional to the square root of the ion temperature T_i and this region is thought to be isothermal.[34] However, these experimental results confirm the supposition that the electron density profiles above 300 km are not in systematic error because the signal bandwidth changes as a function of height. Such an error could occur if the receiver bandwidth were as narrow as or narrower than the signal because then the energy density in the pass band would vary if the spectral width varied with height.

D. Temperature Values

In order to make use of the spectra (Fig. 31) to determine values of the ion temperature T_i, a series of theoretical spectra have been computed for values of the electron-to-ion temperature ratio T_e:T_i in the range 1.0 to 4.0. This work was undertaken by Dr. M. Loewenthal of Group 33 at the author's request. The theory presented by Fejer[3] was employed to calculate the spectra and an IBM 7090 digital computer was used to make the actual computations. The spectra were calculated on the assumption that atomic oxygen is the only ion present and that the radio wavelength λ is ten times the value of the Debye length λ_D (the curves obtained being indistinguishable from those for $\lambda/\lambda_D = \infty$), and are presented in Fig. 34, from which two additional curves are obtained. Figure 35 shows the ratio of the echo power at the peak of the wing to the power at the center frequency as a function of the ratio T_e:T_i. This curve has been used to determine the temperature ratio from experimental data as in Fig. 31. In Fig. 36 the position of the half-power point has been plotted as a function of the temperature ratio T_e:T_i. It can be seen that the bandwidth of the signals increases as the temperature ratio increases. Thus, if the spectral shape is not well known, the variation of the signal bandwidth shown in Fig. 32(a-e) cannot be accurately interpreted as being caused by a variation of T_i alone, the ratio T_e:T_i, or a combination of these effects.

The shapes of the spectra are well-defined for 200 km height and indicate that at all times $T_e = T_i$, i.e., equilibrium prevails. Thus, the small bandwidth variation seen in Fig. 32(a) is the result of equal increases in the electron and ion temperatures during the daytime.

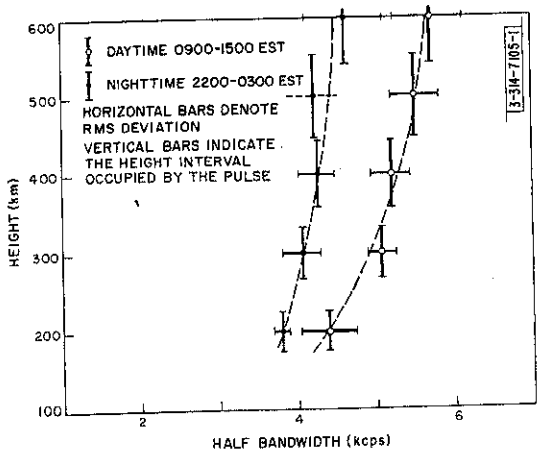

Fig. 33. The average half-bandwidth of the signals plotted as a function of height for nighttime (2200-0300 EST) and daytime (0900-1500 EST) observations.

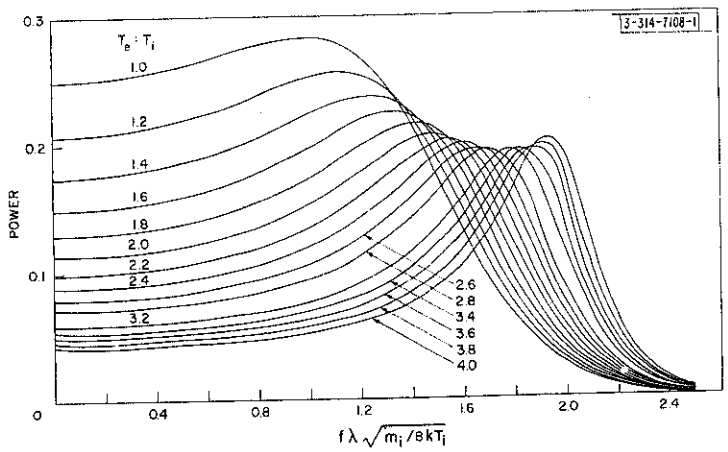

Fig. 34. The power spectra predicted by the theory given by Fejer[6] for electron-to-ion temperature ratios in the range $T_e : T_i = 1.0$ to 4.0. (These curves were computed by Dr. M. Loewenthal.)

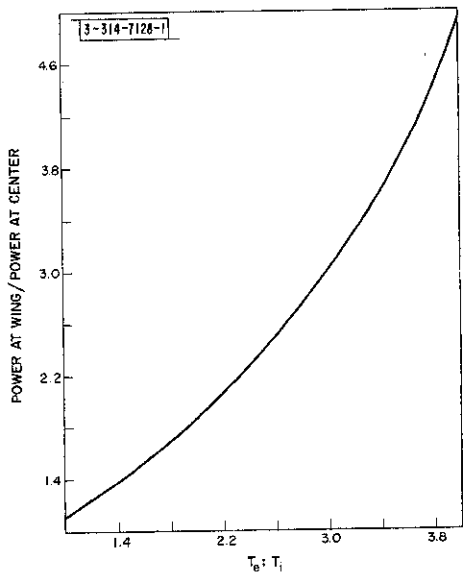

Fig. 35. The ratio of the echo power in the "wing" to that at the center frequency plotted as a function of $T_e : T_i$. These points were obtained from Fig. 34.

The values for the power ratio between the wing and center observed at 300 and 400 km are shown in Fig. 37. It seems clear that at both these heights a power ratio of approximately 1.1:1 exists during the hours of darkness, indicating equilibrium ($T_e = T_i$) as in Fig. 35. During the daytime the value increases roughly in proportion to the sun's altitude, but the scatter of the values is very large, because this measurement is difficult to make. Therefore, it seems impossible to decide whether the diurnal variation observed at 400 km is greater or less than that at 300 km.

At 300 km the quality of the spectra varies because some spectra were obtained by using a 2-msec pulse at a very low elevation (9°) and others with a 1-msec pulse at a much higher elevation (22.5°). The values for the wing-to-center power ratios obtained from each of the spectra have been weighted according to the signal-to-noise ratio (measured at the center frequency), and a weighted mean computed for each hour. These mean values are shown in Fig. 38. The errors shown are the weighted rms deviations. The scatter of the points is quite large and must partly reflect different conditions on the three days (13 to 14 and 26 to 27 March, 1 to 2 April), which have been included in Fig. 38. The right-hand axis of this figure shows the values for the electron-to-ion temperature ratios $T_e:T_i$ corresponding to the power ratios plotted along the left-hand ordinate. It would appear that maximum in the ratio between the temperatures exists just before noon, possibly near 1000 EST. This might be taken as evidence in favor of the second source of atmospheric heating suggested by Harris and Priester.[59] Yet, the results are not sufficiently precise to exclude the possibility that the peak occurs at noon, and that the variation during the day is directly proportional to the sun's altitude. It seems likely that the diurnal variation shown in Fig. 38 will change both with season and with the solar sunspot cycle.

Above 400 km the shape of the profiles is not sufficiently well defined to determine anything but the bandwidth. Thus, in interpreting the results to obtain values for the daytime temperature, we are faced with various possibilities, of which the following represent two extremes:

(1) Above 300 km, T_i may be constant with height, the increase in the bandwidth of the signals being caused solely by an increase in the ratio $T_e:T_i$.

(2) Above 300 km the ratio $T_e:T_i$ may be constant (and follow the variation at 300 km), with the increase in bandwidth caused by an increase in T_i (and a corresponding increase in T_e).

It is possible to reject a third possibility that above 300 km the ratio $T_e:T_i$ rapidly declines to unity, since the ratios of $T_e:T_i$ observed at 400 km are at least as large as those at 300 km. Also, since the collision frequency decreases with height, we might expect the time it takes the electrons to reach equilibrium with the ions to increase rather than decrease. However, this trend can only continue for a limited distance because the solar energy absorbed by the atmosphere also decreases with height.

The temperature distributions corresponding to the two hypotheses (1) and (2) are shown in Fig. 39. Of the two hypotheses, the curves for (2) seem the better choice since, from satellite drag results, a large diurnal variation of the temperature of the neutral particles T_N is known to take place at heights in the order of 500 to 700 km. (It can be presumed that $T_N = T_i$ because of the similar masses of the ions and neutral particles.) The temperatures T_i shown in Fig. 39 for a height of 300 km agree well with the variation assumed in the model developed by Harris and Priester for a 10.7-cm wavelength solar flux of $S \approx 100$ to 150 units.[60] However, the region above 300 km does not seem to be isothermal, as these authors suppose.

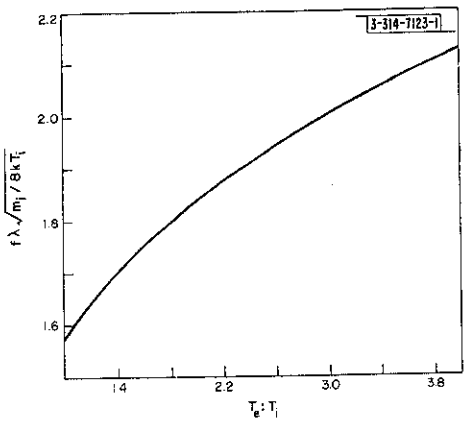

Fig. 36. The position of the "half-bandwidth" point as a function of $T_e : T_i$ (obtained from Fig. 34).

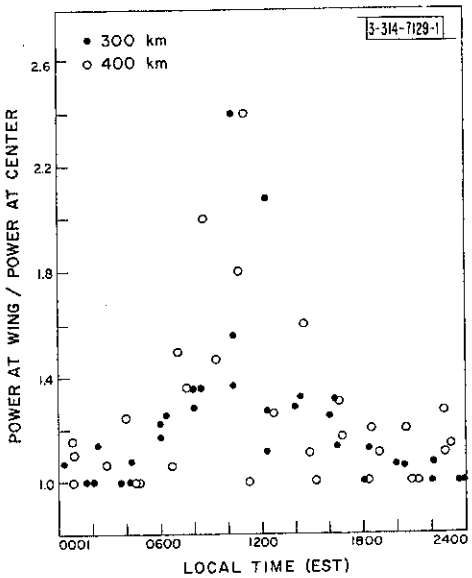

Fig. 37. The observed values for the ratio of the echo power in the "wing" to that at the center frequency for 300 and 400 km height intervals.

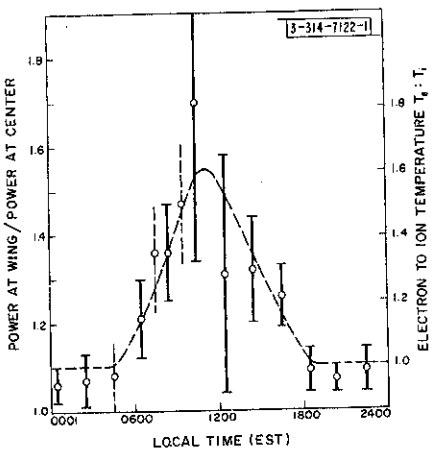

Fig. 38. The rms values for the points given in Fig. 37 for each hourly interval. Shown on the right-hand ordinate is the corresponding scale that gives the ratio between the electron and ion temperatures.

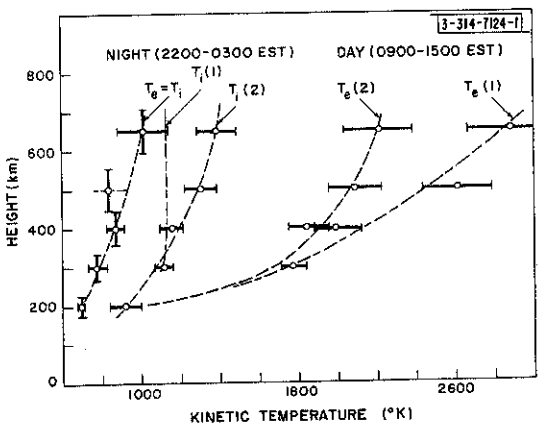

Fig. 39. The temperatures derived from the results of spectrum measurements (e.g., Fig. 31), by means of the curves given in Figs. 35 and 36. The two daytime curves represent the extremes of possible behavior caused by the inability to determine $t_e : T_i$ for altitudes > 400 km.

The large difference between the electron and ion temperatures above 300 km invalidates the attempts of various workers (Van Zandt and Bowles,[61] Hanson and McKibbin,[23] Jackson and Bauer[26] and Evans[16]) to determine the atmospheric temperature from electron density profiles by assuming $T_e = T_i$. Instead, the results demonstrate the existence of the large diurnal variation reported by Serbu, et al.,[58] together with the nonequilibrium conditions first reported by Spencer, et al.[55] The most important feature of the new results seems to be the diurnal variation of the ratio $T_e:T_i$ shown in Fig. 38.

E. Summary of the Spectrum Measurements

The electron and ion temperatures are in equilibrium at all times over the height interval of 170 to 230 km. Somewhat higher, in the region 265 to 335 km, a pronounced departure from equilibrium takes place in the daytime. Evidently, the transition region is quite small. The extent of the nonequilibrium condition could be determined at only 300- and 400-km heights. The wide scatter of values represented by the points makes it impossible to decide whether the effect was any more or less pronounced at 400 than at 300 km. The greatest ratio between the electron and ion temperatures appeared to occur near noon when $T_e:T_i \approx 1.6$. The values for the midday and midnight temperatures T_e and T_i, computed on the assumption that their ratio at 300 km would still hold at 600 to 700 km, are given in Table VI.

TABLE VI
TEMPERATURES DERIVED FROM THE SPECTRUM MEASUREMENTS ACCORDING TO HYPOTHESIS (2)

Height (km)	$T_i = T_e$ (night) °K	T_i (day) °K	T_e (day) °K
200	686 ± 18	920 ± 83	920 ± 83
300	775 ± 48	1230 ± 41	1770 ± 59
400	866 ± 43	1280 ± 64	1840 ± 93
500	838 ± ?	1450 ± 90	2080 ± 130
600/700	1000 ± 110	1530 ± 110	2210 ± 170

IV. ABSOLUTE SCATTERING CROSS SECTION OF THE ELECTRONS

A. Introduction

Gordon[1] gave a value for the scattering cross section of the electrons as

$$\sigma_e = \left(\frac{e^2}{mc^2}\right)^2 \quad \text{in Gaussian units,} \tag{4}$$

and this is the cross section normalized to unit solid angle. Thus, the radar cross section $\sigma_m = 4\pi\sigma_e$. Various theoretical workers[3,6-11] soon showed that, where measurements are conducted at long wavelengths and on the assumption that thermal equilibrium prevails in the ionosphere, σ_m would be only half this value. This is true because the scattering cannot be thought of as taking place from individual electrons but from their collective disturbed behavior caused by the motion of the ions. Under these conditions the expected value for σ_m becomes[56]

$$\sigma_m = 4.99 \times 10^{-29}\ \text{m}^2 \quad . \tag{5}$$

The observed cross section will, however, depend on the electron-to-ion temperature ratio $T_e:T_i$, as can be inferred from the variation of the area under the curves in Figs. 29 and 34. Buneman[27] has discussed this aspect of the problem in some detail, and Fig. 40 shows the variation of σ_m as a function of $T_e:T_i$ obtained from his paper.

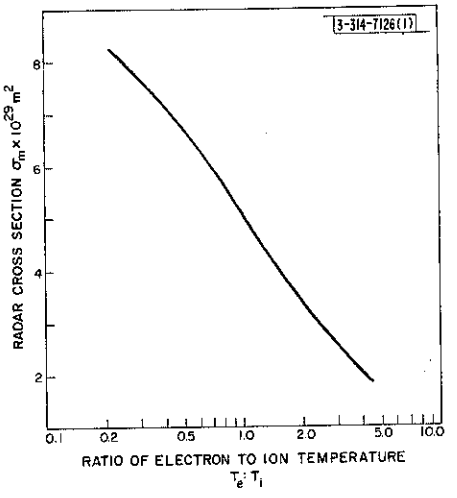

Fig. 40. The theoretical variation of the scattering cross section of an electron as a function of $T_e:T_i$ (after Buneman[27]).

In an early paper Pineo, et al.,[13] gave the misleading impression that the value for the radar cross section σ_m observed at Millstone Radar was in good agreement with the value given by Gordon.[1] This was later corrected by Pineo and Briscoe in Ref. 14, where a value

$$\sigma_m = 1.4 \times 10^{-29} \text{ m}^2 \tag{6}$$

was published.

Bowles[56] has devoted considerable attention to the measurement of the cross section. Provided that a loss between 0.5 and 1.0 db can be attributed to absorption in the lower ionosphere, Bowles obtains values for the cross section σ_m which are in good agreement with the theoretical value in Eq. (5). In addition, he took values for the echo power observed at Millstone by Pineo, et al., and the parameters of the Millstone radar and obtained a value $\sigma_m = 3.6$. This in substantially better agreement with Eq. (5) than that found by Pineo, et al., in Eq. (6). It would seem relevant, therefore, to clear up this discrepancy before proceeding further with the derivation of a new value for σ_m.

B. The Radar Equation for an Extended Target

Bowles[56] has discussed at length the derivation of the radar equation applicable to incoherent backscatter measurements. His account is excellent in its detail, but seems to contain some mistakes. In Eq. (6) of his report the equation for the received echo power P_r is

$$P_r = \frac{P_t \eta_r^2 \sigma c \tau \lambda^2}{128 \pi^3 R^2} \int_\Theta \int_\varphi G^2(\Theta, \varphi) \, d\Theta \, d\varphi \quad ,$$

where the symbols used by Bowles are:

P_t = peak transmitted power (assumed constant within the pulse) in watts,

η_r = efficiency of the feeder system (i.e., over-all resistive losses in the antenna and feed wires),

σ = total cross section per unit volume (m^3)

$= N\sigma_m$.

In these symbols

N = number of electrons/m^3

$= 1.24\, f_o^2 \times 10^{10}$, where

f_o = critical frequency in Mcps;

σ_m = cross section of an electron (Fig. 45);

c = velocity of light (approx. 3×10^8 m/sec);

τ = pulselength (sec);

R = range to the scattering volume;

$G(\Theta\varphi)$ = gain of the antenna over a lossless isotropic radiator at angles Θ and φ, where

Θ = angle measured from the axis of the principal lobe,

φ = azimuth angle of the direction of the ray.

Bowles' Eq. (6) is in error because he has stated (Ref. 56, p. 25) that the total scattering volume within a given incremental solid angle is

$$\frac{c\tau R^2\, d\Theta\, d\varphi}{2} \quad . \tag{7}$$

In the coordinate system adopted by Bowles, Eq. (7) should be

$$\frac{c\tau R^2 \sin\Theta\, d\Theta\, d\varphi}{2} \quad . \tag{8}$$

Thus, Bowles' Eq. (6) should have been stated as*

$$P_r = \frac{P_t \eta_r^2 \sigma c \tau \lambda^2}{128\pi^3 R^2} \int_\Theta \int_\varphi G^2(\Theta\varphi) \sin\Theta\, d\Theta\, d\varphi \quad . \tag{9}$$

For antennas like that employed at Millstone Radar, which has a spherically symmetrical radiation pattern, Eq. (9) now becomes (by integrating φ over 0 to 2π)

$$P_r = \frac{P_t \eta_r^2 \sigma c \tau \lambda^2}{64\pi^2 R^2} \int_\Theta G^2(\Theta) \sin\Theta\, d\Theta \quad . \tag{10}$$

Equation (10) can be developed very simply as follows. Consider a transmitter developing a power P_t driving an isotropic antenna. The total power radiated will be $P_t\eta_r$, and at a distance R the flux density will be

$$\frac{P_t \eta_r}{4\pi R^2} \quad \text{watts/m}^2 \quad . \tag{11}$$

* Note added in proof: The mistake discussed here has since been rectified by the authors. See K.L. Bowles, G.R. Ochs and J.L. Green, "On the Absolute Intensity of Incoherent Scatter Echoes from the Ionosphere," J. Research Natl. Bur. Standards 66D, 395 (1962).

If the antenna is replaced by one having a gain G over an isotropic antenna whose radiation pattern is symmetrical about the axis of the main beam, then in any direction Θ from this axis the flux will be

$$\text{flux} = \frac{P_t \eta_r G(\Theta)}{4\pi R^2} \text{ watts/m}^2 \quad . \tag{12}$$

Now consider the annulus shown in Fig. 41. The flux density across any part of this annulus is stated in Eq. (12). The area of the annulus is $2\pi R^2 \sin\Theta \, d\Theta \, m^2$. The pulse illuminates a region having a depth $c\tau/2$; therefore, provided that $c\tau/2 \ll R$, we may neglect the conical nature of the elemental volume shown in Fig. 41 and write the volume of the element as $R^2 c\tau \sin\Theta \, d\Theta \, m^3$. If N is the electron density per m^3 and it may be assumed that N is slowly changing with height only, this elemental volume contains $\pi R^2 c\tau N \sin\Theta \, d\Theta$ electrons, each of which has a scattering cross section σ_m. Where $N\sigma_m = \sigma$, the total cross section provided by this elemental volume becomes

$$\text{cross section} = \pi R^2 c\tau\sigma \sin\Theta \, d\Theta \quad m^2 \quad . \tag{13}$$

Combining Eqs. (12) and (13), we have for the total intercepted power $0.25 P_t \eta_r G(\Theta) c\tau\sigma \sin\Theta \, d\Theta$ watts, of which a fraction is scattered back to the transmitting antenna where the flux density (watts/m^2) is given by the product of Eq. (13) and $(4\pi R^2)^{-1}$. The flux which falls within the antenna

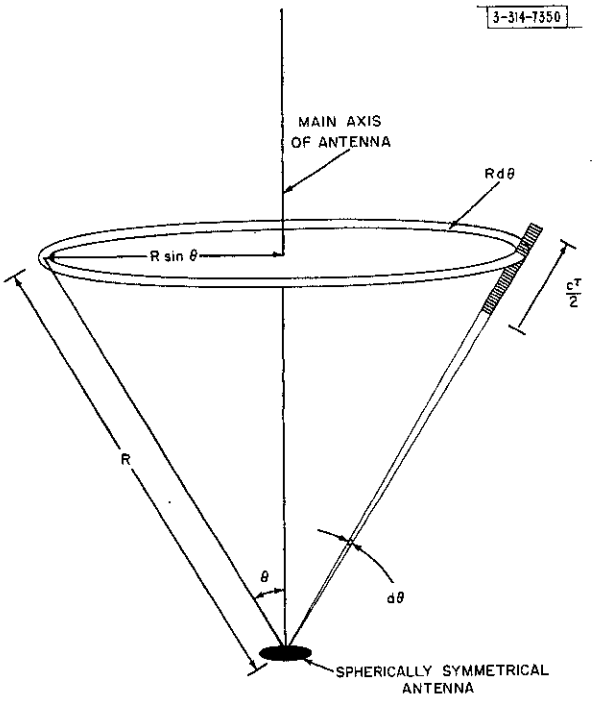

Fig. 41. An elemental annulus lying in the ionosphere at a distance R from the observer.

aperture is (partly) collected and conveyed to the antenna terminals. The collecting (or effective) area of the antenna for radiation at an angle Θ may be written as $A_{eff}(\Theta)$, where

$$A_{eff}(\Theta) = \frac{G(\Theta)\,\lambda^2}{4\pi} \quad . \tag{14}$$

The resistive losses will be present during this process so that the received power from this elemental volume can be written as

$$\text{power} = \frac{P_t \eta_r^2 c\tau\sigma G(\Theta)\, A_{eff}(\Theta)\, \sin\Theta\, d\Theta}{16\pi R^2} \quad \text{watts} \quad . \tag{15}$$

If we now consider all the possible elemental volumes corresponding to all Θ, the total received power P_r obtained is

$$P_r = \frac{P_t \eta_r^2 c\tau\sigma}{16\pi R^2} \int_{\Theta}^{\pi/2} G(\Theta)\, A_{eff}(\Theta)\, \sin\Theta\, d\Theta \quad \text{watts} \quad . \tag{16}$$

By substituting Eq. (14) into (16) it becomes

$$P_r = \frac{P_t \eta_r^2 c\tau\sigma\lambda^2}{64\pi^2 R^2} \int_{\Theta}^{\pi/2} G^2(\Theta)\, \sin\Theta\, d\Theta \quad \text{watts} \quad , \tag{17}$$

which is clearly the same as Eq. (10).

C. Approximate Radar Equation for a Millstone-Type Antenna

In Sec. B we developed a general expression for the radar equation to be employed for an extended target illuminated by a spherically symmetrical antenna. In this section we shall derive an approximate expression for an antenna of the type used at Millstone and compare it with the approximate expressions used by Bowles[56] and Pineo and Hynek.[14]

In Eq. (17) let $G(\Theta)$ be replaced by $G_{\Theta=0}F(\Theta)$, where $G_{\Theta=0}$ is the gain of the antenna measured along the axis ($\Theta = 0$) and $F(\Theta)$ is unity at $\Theta = 0$ and specifies how the gain falls off at other angles. The Millstone aperture has a tapered feed distribution (approximately Gaussian) and the energy falling on the edges of the dish from the horn is about one-tenth of that in the center. The radiation pattern of this antenna is such that the main lobe can be closely represented by a Gaussian function; hence we shall write

$$F(\Theta) = \exp\left[-0.7\Theta^2/\Theta_{1/2}^2\right] \quad , \tag{18}$$

where $\Theta_{1/2}$ is the half beamwidth, i.e., the value for Θ for which $F(\Theta) = 1/2$. Thus, the integral in Eq. (17) becomes

$$I = G_o^2 \int_o^{\pi/2} F^2(\Theta)\, \sin\Theta\, d\Theta$$

$$= G_o^2 \int_o^{\pi/2} \exp\left[-1.4\left(\frac{\Theta}{\Theta_{1/2}}\right)^2\right] \sin\Theta\, d\Theta \quad . \tag{19}$$

By making the transformation $r = R\Theta$ for small Θ, Eq. (19) becomes

$$I \approx \frac{G_o^2}{R^2} \int_o^\infty r \exp\left[-\frac{1.4r^2}{R^2\theta_{1/2}^2}\right] dr \quad . \tag{20}$$

This is the familiar integral $\int_o^\infty x \exp[-a^2x^2]\, dx$ whose solution is $I = 1/2a^2$. Therefore, Eq. (20) yields

$$I \approx \frac{G_o^2\, \theta_{1/2}^2}{2.8} \quad . \tag{21}$$

For this type of antenna,*

$$G_o \approx \frac{7A}{\lambda^2} \quad , \tag{22}$$

where A is the physical aperture. Thus, if we define

$$\eta_A = A_{eff}/A \quad , \tag{23}$$

for this antenna

$$\eta_A \approx 7/4\pi \quad . \tag{24}$$

Also, the beamwidth† is

$$2\theta_{1/2} \approx \frac{70\lambda}{57D} \quad , \tag{25}$$

where D = diameter. If Eq. (22) is written as

$$G_o \approx \frac{7\pi D^2}{4\lambda^2} \quad ,$$

Eq. (21) becomes

$$I \approx G_o \frac{7\pi D^2}{2.8 \times 4\lambda^2} \left(\frac{70\lambda}{114D}\right)^2 \tag{26}$$

$$\approx 0.74\, G_o \quad . \tag{27}$$

Actual substitution in Eq. (21) of the measured values for $\theta_{1/2}$ and G_o of the Millstone antenna yields $I = 0.76\, G_o$. Therefore, Eq. (17) becomes

$$P_r = 0.76 \frac{P_t \eta_r^2 c\tau\sigma\lambda^2}{64\pi^2 R^2} G_o \quad \text{watts} \quad , \tag{28}$$

or

$$P_r = 0.76 \frac{P_t \eta_r^2 c\tau\sigma A_o}{16\pi R^2} \quad \text{watts} \quad . \tag{29}$$

---

* Reference Data for Radio Engineers, p. 700.

† Ibid.

Pineo and Hynek[14] have used this equation without the factor 0.76; hence, we should expect values for σ_m derived by these authors to be a factor of 0.76 of the true values.

Bowles[56] has considered the effect of power radiated into the sidelobes, which is largely wasted. He defines an efficiency factor η_s as being the ratio of the power in the main lobe to the total power radiated. Thus, his approximate Eq. (29) contains a term η_s^2 to account for this factor. Power which is radiated at some angle $\Theta > \Theta_{max}$ may rightly be regarded as wasted since the ionosphere does not form a hemisphere above the observer. Therefore, in Eq. (17) the upper limit of the integral sign ($\pi/2$) should be replaced by some lesser value of Θ_{max}. Then Bowles' term η_s^2 would be given by

$$\eta_s^2 = \frac{\int_0^{\Theta_{max}} G^2(\Theta) \sin\Theta \, d\Theta}{\int_0^{\pi/2} G^2(\Theta) \sin\Theta \, d\Theta} \quad . \tag{30}$$

This definition differs from that given by Bowles. The exact value of Θ_{max} is debatable. Bowles apparently takes the view that only power in the main lobe is useful, although for narrow-beam antennas such as the one employed by him ($\Theta_{1/2} = 1°/2$) and the one used by Pineo ($\Theta_{1/2} = 1°$), the power contained in the sidelobes adjacent to the main lobe is not wasted. It is evident that no simple criterion to determine Θ_{max} can be laid down, but, as an order of magnitude, Θ_{max} may be taken as approximately 10 to 20° for narrow-beam antennas. It should be made clear that the term η_s is warranted only by the extended nature of the target. No such term is present in the case of a point target as can be seen in Eq. (30) where, for such a target, the upper limit to the integrals $\to 0$ and $\eta_s \to 1$. It is equally true that η_s cannot be determined from radar observations of a point target. This conclusion brings us to the second confusing part of Bowles' development. Bowles apparently believes that even for a point target (e.g., a radio star) the received power is proportional to $\eta_A \eta_s A$ and, since this is a common way to measure the antenna efficiency, one actually measures the product $\eta_A \eta_s$. Thus, in his report* Bowles states that for Millstone, where the antenna efficiency is 35 percent (the true value is nearer 40 percent), "$\eta_A \eta_s = 0.35$ and if η_A is assumed to be 0.6 $\eta_s \sim 0.58$." Since η_s^2 occurs in the final equation, this is a large effect. We labor this point (and indeed the whole of the preceding discussion) because the differences between the results of Pineo and Bowles center around the term η_s and how it is determined. Pineo and Hynek[14] have included no such term in their analysis, believing that $\eta_s \to 1$ for a Millstone-type antenna, so that their value for σ_m is about one-third of the value which Bowles obtains from the same data.

D. Values of η_A, η_r and η_s for Millstone Radar

The total two-way feedline losses given in Table I are 2 db. Hence, $\eta_r^2 = 0.63$. A value of 0.40 for η_A can be obtained from the ratio of the effective aperture (210 m^2) to the physical aperture (520 m^2). This value is low compared to the efficiency stated in Eq. (24) and arises as a result of attempts to minimize the large sidelobe introduced by the feed support structure by using a feed system which provides more than a 10-db taper of the primary illumination pattern.[62] This is necessary for tracking operations but unnecessary for backscatter measurements. The net effect is to decrease η_A and increase η_s, though the increase in the latter is insufficient to

* Page 35.

offset the decrease in η_A. The value for the effective aperture (Table I) is consistent with both absolute gain measurements [Eq. (14)] and observations of intense radio stars.

A value for η_s is more difficult to arrive at. It will be noted that, as defined in Eq. (30), it depends upon the square of the gain integrated between 0 and Θ_{max}. Unfortunately, the contour plots for the Millstone antenna given by Fritsch[62] do not cover a sufficiently wide range of angles to permit η_s to be determined. Instead, we shall derive an approximate value using results obtained by Ricardi.[63] Ricardi has shown that if the antenna radiation pattern is broken into two parts, a main lobe and an isotropic component, the peak intensity ratio between these two can be found as follows:

$$\frac{\text{gain at the peak of the main beam}}{\text{isotropic component}} = \frac{m G_o}{m - 1} \quad , \tag{31}$$

where

$$m = \frac{\text{ideal gain } G_i}{\text{observed gain } G_o} \quad , \tag{32}$$

in which the ideal gain G_i is given as

$$G_i = \frac{13(\Theta_{1/2})^2}{4} \quad . \tag{33}$$

For the Millstone antenna the beamwidth $2\Theta_{1/2} = 2.1°$ (0.369 radian); hence, the ideal gain, obtained from Eq. (33), is 9544. The observed gain (corresponding to 37.5 db) is 5623, which yields $m \approx 1.7$ in Eq. (32). Thus, the ratio $(m/m - 1) = 2.4{:}1$, and the ratio between the peak of the main beam and the average sidelobe level is approximately 41.3 db. The ratio between the square of these numbers is 82.6 db, and this is so large that η_s^2 is indistinguishable from unity.

A check on this conclusion was performed by computing the integral

$$I = \int_o^{\Theta_{max}} F^2(\Theta) \sin\Theta \, d\Theta \tag{34}$$

for the antenna pattern of a scale model of the new 200-ft parabolic antenna presently under construction at Millstone Hill. This antenna has a half-power beamwidth $2\Theta_{1/2} = 0.74°$ (0.0067 radian), and for this value Eq. (34), integrated numerically to $\Theta_{max} = 1°$, yielded $I' = 0.0008243$ steradian. When the integral was re-evaluated for angles up to $\Theta_{max} = 4°$, a value $I'' = 1.00012\ I'$ was obtained, and when $\Theta_{max} = 60°$, then $I''' = 1.00014\ I'$. Clearly, there is little difference between values of the integral computed for $1° < \Theta_{max} < 90°$. It follows that $\eta_s^2 = 1$ and that Pineo and Hynek were right to ignore this term.

The result given in Eq. (21) for the solution of the integral in Eq. (17) has also been checked by integrating numerically over the actual antenna pattern of the Millstone antenna.[62] The result obtained,

$$I = \frac{G_o \Theta_{1/2}^2}{2.83} \quad , \tag{35}$$

is so close to the solution given in Eq. (21) that Eq. (29) can be taken as the correct equation to use for the observations reported here. Equation (29) may be rewritten as

$$P_r = \frac{0.76\eta_r^2 P_t c\tau A_{eff}(1.24 \times 10^{10})\, f_o^2 \sigma_m}{16\pi R^2} \quad \text{watts} \quad ; \tag{36}$$

therefore,

$$\frac{P_r R^2}{f_o^2} = \frac{0.76\eta_r^2 P_t c\tau A_{eff}(1.24 \times 10^{10})\, \sigma_m}{16\pi} \quad \text{mks} \quad . \tag{37}$$

By setting $P_r = P_d b$, where P_d is the power density (watts/cps) and b is the effective bandwidth of the signal, and introducing the parameters given in Table I, Eq. (37) becomes

$$\frac{P_d R^2 b}{f_o^2} = \frac{0.76\eta_r^2 P_t c\tau A_{eff}(1.24 \times 10^{10})\, \sigma_m}{16\pi} \quad \text{mks} \tag{38}$$

$$= 0.82 \times 10^{22} \sigma_m \quad \text{mks} \quad . \tag{39}$$

The effective bandwidth b for most height intervals (Fig. 33) during the daytime is approximately 11 kcps. Hence,

$$\sigma_m = 1.34 \times 10^{-18} \frac{P_d R^2}{f_o^2} \quad \text{m}^2 \quad . \tag{40}$$

E. An Average Value for σ_m

In Eq. (39) we have grouped all the variable quantities on the left-hand side of the equation. The computer program for the electron density profile calculates the value of $P_d R^2$ corresponding to each point and multiplies these values by 10^{14} so that they appear as a four- to five-digit number. The values obtained corresponding to N_{max} for the profiles shown in Sec. II have been plotted as a function of f_o^2 in Fig. 42 for those measurements that were made using the 11-kcps receiver bandwidth. The Ft. Belvoir values for f_o were used throughout. It can be seen that although the normalized power density $P_d R^2$ does increase as f_o^2 increases, there is a wide scatter of values. The mean value for $P_d R^2 / f_o^2$ for all points shown in Fig. 42 is 1.35×10^{-11} mks, which, when inserted into Eq. (40) yields a value $\sigma_m \sim 1.81 \times 10^{-29}$ m^2.

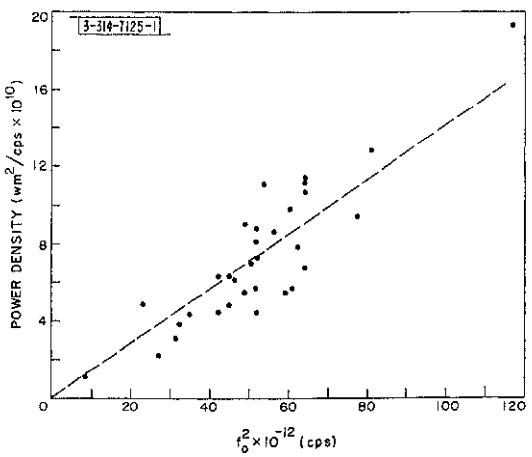

Fig. 42. The variation of the product of the power density P_d of the reflected signals and the square of the range R^2 as a function of the square of the F2 layer critical frequency f_o. The values for $P_d R^2$ correspond to the peak of the layer and were obtained for all the profiles shown in Figs. 3 through 17 where a receiver bandwidth of 11 kcps had been employed. The values for f_o are those obtained at Ft. Belvoir (B).

There are several sources of error in the above value. Presumably, there are systematic errors in the estimation of the transmitter power P_t, the effective antenna aperture A_{eff}, the feeder losses η_r and possibly the method of calibrating the receiver. An outside limit on each of these values would be approximately ±0.5 db, so that the probable error would be approximately ±1 db. Also, there are errors of measurement of both P_d and f_o. Undoubtedly these are partly responsible for the scatter of the points in Fig. 42, although small changes in P_t from one run to the next may make a contribution. Variations of $T_e:T_i$ must also contribute somewhat to the scatter in the values.

Two systematic errors which act to reduce the observed value for σ_m deserve comment. The first is the error in the profile for the electron density due to the convolution of the pulse with the true distribution. This error, which is most serious in the vicinity of N_{max}, has been discussed in Sec. II. By observing the trend of the electron density vs pulselength (actually antenna elevation) such as that shown in Fig. 3, it can be estimated that the observed density at N_{max} may be only 90 percent of the true value, even for observations at 15° elevation. The second error arises from the use of an equivalent bandwidth b in Eq. (38). Figure 43 shows the actual response of the filter used in the receiver for all the measurements made with a receiver bandwidth of 11 kcps. By convolving this response curve with the actual echo power distribution (e.g., Fig. 31), one can examine the effect of the filter on the spectrum. The filter bandwidth has been chosen to maximize the signal-to-noise ratio, but is by no means a perfect match to the signal spectrum. The observed signal-to-noise ratio, therefore, appears to be approximately 80 percent of that which would be obtained with an ideal filter. These two systematic errors act in a manner which would cause σ_m to be underestimated, and have a value of only 70 ± 10 percent of the true value during the daytime.

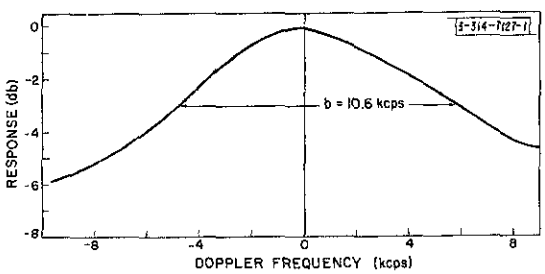

Fig. 43. The response curve for the matched "11-kcps" filter employed in the receiver.

Finally, in view of the variation of σ_m with the temperature ratio $T_e:T_i$ we might expect, on the basis of the spectrum measurements, that σ_m will exhibit a diurnal variation. In order to look for this it was considered necessary to correct for the effect of the convolution of the pulse with the true distribution. Accordingly, the values for N_{max} shown in Fig. 3 were plotted against the effective pulse length and the relationship obtained was found to be linear. This law could be extrapolated to yield the value of N_{max}, which might have been observed with an exceedingly short pulse. The correction factors derived from this relation are given in Table VII. For analysis we chose values for the product P_dR^2 corresponding to the peak electron density on each of the profiles shown in Figs. 4 through 18, where an 11-kcps receiver bandwidth was employed. These values were scaled up according to Table VII, and increased by a factor 1.25 to allow for the mismatch between the signal spectrum and the receiver filter. Finally, these corrected values were used to provide values for σ_m by use of Eq. (40). The average values for σ_m for each hourly interval over the day are given in Table VIII. It can be seen that, although there is a slight tendency

TABLE VII

CORRECTION FACTORS FOR VALUES FOR N_{max} PLOTTED AGAINST PULSE LENGTH

Elevation Angle	Correction Factor
90°	1.433
60°	1.365
45°	1.274
30°	1.212
20°	1.146
15°	1.116

TABLE VIII

AVERAGE VALUES FOR σ_m

Local Time (EST)	Mean Value of σ_m ($\times 10^{-29}$ m^2)	rms Deviation
07 – 08	1.57	(single value)
08 – 09	2.94	$\pm 0.238 \times 10^{-29}$ m^2
09 – 10	2.67	$\pm 0.99 \times 10^{-29}$ m^2
10 – 11	2.72	$\pm 0.71 \times 10^{-29}$ m^2
11 – 12	3.73	(single value)
12 – 13		
13 – 14	2.72	$\pm 0.35 \times 10^{-29}$ m^2
14 – 15	2.41	$\pm 0.42 \times 10^{-29}$ m^2
15 – 16	3.12	$\pm 0.49 \times 10^{-29}$ m^2
16 – 17	3.20	$\pm 0.77 \times 10^{-29}$ m^2
17 – 18		
18 – 19		
19 – 20	3.27	(single value)

TABLE IX

VALUES FOR THE ION TEMPERATURE T_i DEDUCED FROM THE SCALE HEIGHT MEASUREMENTS (Sec. II) ASSUMING $T_e = 1.6\ T_i$

True Height (km)	Winter Day (0900 – 1500 EST) (°K)	Summer Day (1000 – 1400 EST) (°K)
400	783	1090
500	980	1320
600	1100	1530
700	1220	1740

for σ_m to decrease near midday (as might be expected), the rms deviations of the points are too large for this result to be regarded as conclusive. Presumably the large experimental errors tend to mask whatever variation may exist. A weighted mean value for σ_m obtained from Table IX for the hours 0800 to 1700 EST is $\sigma_m = 2.82 \pm 0.49 \times 10^{-29}\ m^2$. The ±1 db uncertainty as to the equipment parameters increases the probable error, so that the final result for the average daytime value for σ_m is

$$\sigma_m = 2.8 \pm 0.8 \times 10^{-29}\ m^2 \quad . \tag{41}$$

This value is somewhat lower than would be expected for a maximum temperature ratio $T_e:T_i = 1.6$, for which the average daytime value of σ_m would be $\sim 4 \times 10^{-29}\ m^2$. It seems possible that the discrepancy could be resolved if the temperature ratio $T_e:T_i$ were higher than 1.6 during 1960-61. A value for $T_e:T_i$ of 2 or more, as suggested by Pineo and Hynek,[29] would bring the observed and expected cross sections into closer agreement.

F. Summary

We have derived a radar equation applicable to backscatter observations made with a circularly symmetrical beam. We have seen that Eq. (29) differs from that employed by Pineo and Hynek by a factor of 0.76, and from that used by Bowles for the Millstone Radar by a factor of $0.76\ \eta_s^2$. Bowles has argued that, for Millstone, $\eta_s^2 = 0.33$ and we have shown that this conclusion is incorrect. For a parabola with a tapered feed, η_s^2 is indistinguishable from unity.

We have employed the radar equation together with the results reported in Sec. II to obtain an average daytime value $\sigma_m = 2.8 \pm 0.8 \times 10^{-29}\ m^2$ for the period reported. This average is somewhat lower than expected for electrons at a temperature $T_e = 1.6\ T_i$, but is compatible with a value $T_e = 2\ T_i$. Even after an attempt was made to correct the values of N_{max} for the different elevations employed in the measurements, no systematic variation of σ_m during the daytime was evident.

V. CONCLUSION

From results for the density distribution of the electrons above N_{max} (summarized in Tables III and IV) and those of the spectrum measurements (Table VI), we have seen that the variation of the bandwidth of the signals above h_{max} is small and hence cannot be a factor influencing the density distribution. The departure from equilibrium conditions near midday will, however, cause a distortion in the electron density profiles obtained near this time.

It is clear from the remarks in Sec. III that the values for the scale height of the neutral particles derived from Table IV and plotted in Fig. 28 by assuming both diffusive equilibrium and temperature equilibrium ($T_e = T_i$) are in error. The correct values will be somewhat lower, but in view of the probable dependence of the electron-to-ion temperature ratio on the sunspot cycle, a proper correction factor cannot easily be applied. We may, however, reinterpret the scale height measurements by making the same set of assumptions that have been made in the temperature measurements to see if they are consistent. Table IX gives the temperatures derived from the scale height measurements (Table IV) when the following assumptions are made:

(a) The scale height H_i is related to the electron and ion temperatures by Eq. (3),

$$H_i = \frac{k(T_e + T_i)}{m_i g} ,$$

i.e., diffusive equilibrium is in operation.

(b) The ratio T_e:T_i appropriate to the values for the scale height observed in the period closest to midday is 1.6:1 for both summer and winter at all heights above 300 km.

(c) Oxygen is the principal ion.

Assumptions (b) and (c) are in essence contained in the derivation of the temperatures from the spectrum measurements (Table VI). Thus, agreement between Tables VI and IX would support assumption (a).

As shown in Fig. 44 where these temperature values for T_i are plotted, the agreement between the temperatures derived by the two methods is poor. At first sight, it would seem that this does not necessarily invalidate assumption (a), because the effect of the ratio T_e:T_i [assumption (b)] on the two measurements is different. The ratio T_e:T_i has little effect on the value

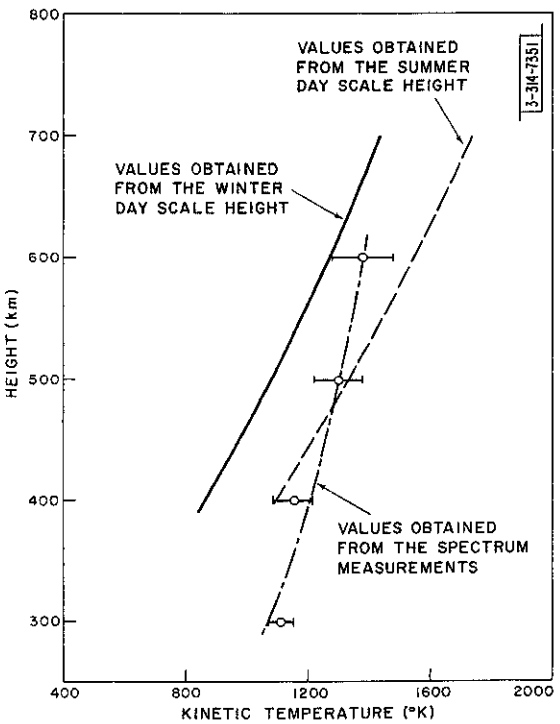

Fig. 44. This figure provides a comparison of the temperatures deduced directly from the spectral measurements and those obtained from the scale height measurements after making certain assumptions listed in the text.

for T_i derived from the spectrum measurements in Fig. 36. By varying this parameter the temperatures deduced from the scale height measurements can be adjusted. It seems likely that there will be marked seasonal variations in T_i, and we should not expect the three curves in Fig. 44 to be superimposed, though we might expect that they would have similar slopes. This would require that T_e:T_i increase with height [in agreement with hypothesis (b) in Sec. III-D]. However, such an increase would cause the scattering cross section σ_m to decrease in proportion, so that the over-all density profile cannot be adjusted by large amounts in this way. Consequently, we are forced to conclude that unless the measurements are subject to serious systematic errors, they imply that the region above h_{max} up to about 600 to 700 km is not in diffusive equilibrium.

ACKNOWLEDGMENT

The author wishes to acknowledge the cooperation and encouragement received from Dr. G.H. Pettengill, Leader of Group 314, and from Mr. V.C. Pineo, Assistant Group Leader. Thanks are also due to Dr. M. Loewenthal (then in Group 33), who arranged for the computation of the curves shown in Fig.34. W.A. Reid, who assisted in the construction and subsequent operation of the spectrum analyzer described in Sec. III-B, deserves special credit, as do many other members of the Millstone Radar staff, too numerous to mention here, who were concerned with routine operation of equipment for the electron density measurements. Finally, the author is indebted to J.F. MacLeod and Mrs. Mary Anderson, who performed most of the data reduction.

REFERENCES

1. W.E. Gordon, "Incoherent Scattering of Radio Waves by Free Electrons with Applications to Space Explorations by Radar," Proc. IRE 46, 1824 (1958).
2. Lord Rayleigh, "On the Light from the Sky, its Polarization and Colour," Phil. Mag. Ser. 4 41, 107 (1871).
3. J.S. Fejer, "Scattering of Radio Waves by an Ionized Gas in Thermal Equilibrium in the Presence of a Uniform Magnetic Field," Can. J. Phys. 39, 716 (1961).
4. K.L. Bowles, "Observations of Vertical Incidence Scatter from the Ionosphere at 41 Mcps," Phys. Rev. Letters 1, 454 (1958).
5. _____, "Incoherent Scattering by Free Electrons as a Technique for Studying the Ionosphere and Exosphere: Some Observations and Theoretical Considerations," J. Research Natl. Bur. Standards 65D, 1 (1961); see also NBS Report No. 6070 (1959).
6. J.A. Fejer, "Scattering of Radio Waves by an Ionized Gas in Thermal Equilibrium," Can. J. Phys. 38, 1114 (1960).
7. D.T. Farley, J.P. Dougherty and D.W. Barron, "A Theory of Incoherent Scattering of Radio Waves by a Plasma. II. Scattering in a Magnetic Field," Proc. Roy. Soc. (London) A263, 238 (1961).
8. J.P. Dougherty and D.T. Farley, "A Theory of Incoherent Scattering of Radio Waves by a Plasma," Proc. Roy. Soc. (London) A259, 79 (1960).
9. T. Hagfors, "Density Fluctuations in a Plasma in a Magnetic Field, with Applications to the Ionosphere," J. Geophys. Res. 66, 1699 (1961).
10. E.E. Salpeter, "Scattering of Radio Waves by Electrons Above the Ionosphere," J. Geophys. Res. 65, 1851 (1960).
11. _____, "Electron Density Fluctuations in a Plasma," Phys. Rev. 120, 1528 (1960).
12. V.C. Pineo, L.G. Kraft and H.W. Briscoe, "Ionospheric Backscatter Observation at 440 Mcps," J. Geophys. Res. 65, 1620 (1960).
13. _____, "Some Characteristics of Ionospheric Backscatter Observed at 440 Mcps," J. Geophys. Res. 65, 2629 (1960); see also G-Report 30G-0008, Lincoln Laboratory, M.I.T. (6 July 1960), ASTIA 239487.
14. V.C. Pineo and H.W. Briscoe, "Discussion of Incoherent Backscatter Power Measurements at 440 Mcps," J. Geophys. Res. 66, 3965 (1961); see also G-Report 30G-0013, Lincoln Laboratory, M.I.T. (5 June 1961), not generally available.
15. V.C. Pineo, L.G. Kraft, H.W. Briscoe and D.P. Hynek, "Experimental Studies of the F-Region Using the Incoherent Backscatter Technique at Frequencies Around 400 Megacycles," Conference Paper presented at the URSI Spring Meeting, Washington (1961).
16. J.V. Evans, "Distribution of Electrons in the F-Region," G-Report 30G-0014, Lincoln Laboratory, M.I.T. (15 September 1961), ASTIA 263902, H-345.
17. G.H. Pettengill and L.G. Kraft, "Earth Satellite Observations made with the Millstone Hill Radar," Avionics Research (Pergamon Press, Oxford, 1958), p.125.
18. J.S. Arthur, J.C. Henry, G.H. Pettengill and P.B. Sebring, "The Millstone Radar in Satellite and Missile Tracking," Ballistic Missiles and Space Technology, Vol. III (Pergamon Press, Oxford, 1961), p.81.
19. G.H. Millman, A.J. Moceyunas, A.E. Sanders and R.F. Wyrick, "The Effect of Faraday Rotation on Incoherent Backscatter Observations," J. Geophys. Res. 66, 1564 (1961).
20. G.H. Millman, V.C. Pineo and J.W. Wright, "Observations of Ionospheric Effects by Incoherent Backscatter Techniques," Conference Paper presented at the URSI Spring Meeting, Washington (1961).
21. J.S. Nisbet, "Electron Density Distribution in the Upper Ionosphere from Rocket Measurements," J. Geophys. Res. 65, 2595 (1960).

22. J.S. Nisbet and S.A. Bowhill, "Electron Densities in the F-Region of the Ionosphere from Rocket Measurements, Part II, Results of Analysis," J. Geophys. Res. 65, 3609 (1960).

23. W.B. Hanson and D.D. McKibbin, "An Ion Trap Measurement of the Ion Concentration Profile Above the F2 Peak," J. Geophys. Res. 66, 1667 (1961).

24. W.W. Berning, "A Sounding Rocket Measurement of Electron Densities to 1500 Kilometers," J. Geophys. Res. 65, 2589 (1960).

25. _____, Conference Paper presented at the URSI Spring Meeting (1961).

26. J.E. Jackson and S.J. Bauer, "Rocket Measurement of a Daytime Electron-Density Profile up to 620 Kilometers," J. Geophys. Res. 66, 3055 (1961).

27. O. Buneman, "Scattering of Radiation by the Fluctuations in a Non-Equilibrium Plasma," J. Geophys. Res. 67, 2050 (1962).

28. H.G. Booker, "A Theory of Scattering by Nonisotropic Irregularities with Application to Radar Reflections from the Aurora," J. Atmos. Terr. Phys. 8, 204 (1956).

29. V.C. Pineo and D.P. Hynek, "Diurnal Variation of the Spectral Width Shape and Other Characteristics of Incoherent Ionospheric Backscatter Observed at 440 Mcps During a 24-Hour Period in May 1961," Conference Paper presented at the AGU Meeting, Los Angeles (1961) and at the URSI Meeting, Washington (1962).

30. N.M. Bryce, "Variations in Ionospheric F-Region Characteristics," Australian J. Phys. 11, 587 (1958).

31. S. Chapman, "The Absorption and Dissociative or Ionizing Effect of Monochromatic Radiation in an Atmosphere on a Rotating Earth," Proc. Phys. Soc. 43, 26 (1931).

32. F.S. Johnson, "The Ion Distribution Above the F2 Maximum," J. Geophys. Res. 65, 577 (1960).

33. T.J. Yonezawa, "A New Theory of the F2 Layer," J. Radio Research Laboratories (Japan) 11, 1 (1956).

34. M. Nicolet, "Structure of the Thermosphere," Planet. Space Sci. 5, 1 (1961).

35. F.S. Johnson, The Satellite Environment Handbook (Stanford University Press, Stanford, 1961), p.13.

36. T. Yonezawa, "On the Physical Properties and Composition of the Upper Atmosphere Between 100 and 400 Kilometers above Ground in Middle Latitudes," J. Radio Research Laboratories (Japan) 7, 69 (1960).

37. H.K. Kallman-Bijl, "Daytime and Nighttime Atmospheric Properties Derived from Rocket and Satellite Observations," J. Geophys. Res. 66, 787 (1961).

38. _____, "Variable Atmospheric Properties Derived from Rocket and Satellite Observations," J. Atmos. Terr. Phys. 23, 330 (1961).

39. R.A. Minzner, K.S.W. Champion and M.L. Pond, "The ARDC Model Atmosphere 1959," Air Force Cambridge Research Center Technical Report 59-267 (1959).

40. D.G. King-Hele and D.M.C. Walker, "Upper Atmosphere Density During the Years 1957-1961, Determined from Satellite Orbits," Conference Paper presented at the COSPAR Meeting, Florence (1961).

41. L.G. Jacchia, "A Variable Atmospheric Density Model from Satellite Accelerations," J. Geophys. Res. 65, 2775 (1960).

42. J.V. Evans and G.N. Taylor, "The Electron Content of the Ionosphere in Winter," Proc. Roy. Soc. (London) A 263, 189 (1961).

43. J.C. Seddon (private communication).

44. G.N. Taylor (private communication).

45. G.H. Millman and F. Rose, "A Study of Ionospheric and Lunar Characteristics by Radar Techniques," General Electric Company, TIS R61EMH40 (1961).

46. V.C. Pineo and D.P. Hynek, "Geomagnetic Effects on the Frequency Spectrum of Incoherent Backscatter Observed at 425 Mc/s at Trinidad, T.W.I.," Conference Paper presented at the AGU Meeting, Los Angeles (1961) and at the URSI Meeting, Washington (1962).

47. J. Renau, H. Camnitz and W. Flood, "The Spectrum and the Total Intensity of Electromagnetic Waves Scattered from an Ionized Gas in Thermal Equilibrium in the Presence of a Static Quasi-Uniform Magnetic Field," J. Geophys. Res. 66, 2703 (1961).

48. M. Rishbeth, "Atmospheric Composition and the F Layer of the Ionosphere," Planet. Space Sci. 9, 149 (1962).

49. S.M. Poloskov, "Upper Atmosphere Structure Parameters According to Data Obtained from USSR Rockets and Satellites During IGY," Space Research, H.K. Kallmann-Bijl, ed. (North Holland Publishing Co., Amsterdam, 1960), p.95.

50. V.G. Istomin, "Investigation of the Earth's Atmosphere on Geophysical Rockets 1957-1959," Planet. Space Sci. 9, 179 (1962).

51. M. Nicolet, "Helium an Important Constituent in the Lower Exosphere," J. Geophys. Res. 66, 2263 (1961).

52. S.J. Bauer, "The Electron Density Distribution above the F_2 Peak and Associated Atmospheric Parameters," J. Atmospheric Sci. 19, 17 (1962).

53. S.J. Bauer and J.E. Jackson, "Rocket Measurement of the Electron-Density Distribution in the Topside Ionosphere," J. Geophys. Res. 67, 1675 (1962).

54. J.A. Ratcliffe and K. Weekes, "The Ionosphere," Physics of the Upper Atmosphere, J.A. Ratcliffe, ed. (Academic Press, London, 1960), p. 445.

55. N.W. Spencer, L.M. Brace and G.R. Carignan, "Electron Temperature Evidence for Non-Thermal Equilibrium in the Ionosphere," J. Geophys. Res. 67, 157 (1962).

56. K.L. Bowles, "Progress Report No.2, Lima Radar Observatory," Natl. Bur. Standards Report 7208 (1961); also Conference Paper presented at the URSI Meeting, Washington (1962).

57. F.S. Johnson (private communication).

58. G.P. Serbu, R.E. Bourdeau and J.L. Donley, "Electron Temperature Measurements on the Explorer VIII Satellite," J. Geophys. Res. 66, 4313 (1961).

59. I.Harris and W. Priester, "Time-Dependent Structure of the Upper Atmosphere," Conference Paper presented at the COSPAR Meeting, Washington, 1962. Also NASA Goddard Space Flight Center Report (12 April 1962).

60. _____, "Theoretical Models for the Solar-Cycle Variation of the Upper Atmosphere," NASA Goddard Space Flight Center Report (24 April 1962).

61. T.E. Van Zandt and K.L. Bowles, "Use of the Incoherent Scatter Technique to Obtain Ionospheric Temperature," J. Geophys. Res. 65, 2627 (1960).

62. P.C. Fritsch, "Final Technical Report – Antenna and RF Circuit Design – Millstone Hill Radar," Technical Report No. 193, Lincoln Laboratory, M.I.T. (1959), ASTIA 305217.

63. L.J. Ricardi, "Large Antenna Design," Lecture, M.I.T. Summer Session on Problems of High-Power Radar Design (31 July – 11 August 1961).